Vysoká škola báňská – Technická univerzita Ostrava
Univerzitní studijní programy

Synthesis and characterization of polypyrrole layers on different substrates

Syntéza a charakterizace polypyrrolových vrstev na různých substrátech

Autor: Bc. Hana Koníčková

Vedoucí diplomové práce: doc. Ing. Lenka Kulhánková, Ph.D.

Datum odevzdání: 21. 5. 2018

VŠB - Technical University of Ostrava
University Study Programmes
CNT - Nanotechnology Centre

Diploma Thesis Assignment

Student: **Bc. Hana Koníčková**

Study Programme: N3942 Nanotechnology

Study Branch: 3942T001 Nanotechnology

Title: Synthesis and characterization of polypyrrole layers on different substrates
Syntéza a charakterizace polypyrrolových vrstev na různých substrátech

The thesis language: English

Description:

During the processing of this master's thesis, the student will acquire theoretical and practical knowledge about the technology of preparation of thin polypyrrole layers synthesized prepared on different substrates under different conditions in order to achieve high homogeneity and electrical conductivity of the layers. Concurrently with the preparation, the work on this master's thesis will also include the measurement of the electrical conductivity of the layers, their structural characterization, and study on how parameters affect the structure and the conductivity. Within the framework of the structural characterization, the student will also focus on the construction and optimization of atomic models, in order to clarify the arrangement of polypyrrole chains in the layers deposited on experimentally tested substrates.

1. To find and read literature on an assigned topic.
2. Preparation of polypyrrole layers.
3. Structure characterization of the prepared layers.
4. Measurement of electrical conductivity of prepared layers.
5. Preparation and geometry optimization of atomistic models of polypyrrole chains anchored on different substrates.
6. Evaluation of the optimal conditions for preparation of polypyrrole layers in terms of the highest electrical conductivity.

References:

Jatratkar A. A., Yadav J. B., Kamat S. V., Patil V. S., Mahadik D. B., Barshilia H. C., Puri V., Puri R. K.: Consequence of oxidant to monomer ratio on optical and structural properties of polypyrrole thin film deposited by oxidation polymerization technique. Journal of Physics and Chemistry of Solids 80 (2015), 78-83.

Hinchcliffe A.: Molecular Modeling for Beginners. Second Edition. John Wiley & Sons Ltd, United Kingdom (2008). ISBN 978-0-470-51313-2.

Sun H., COMPASS: An ab Initio Force-Field Optimized for Condensed-Phase Applications - Overview with Details on Alkane and Benzene Compounds. The Journal of Physical Chemistry B 102 (1998) 7338-7364.

Rappé A. K, Casewit C. J, Colwell K. S, Goddard W. A., Skiff W. M.: UFF a full periodic table force field

for molecular mechanics and molecular dynamics simulations. Journal of the American Chemical Society 114 (1992) 10024-10035.

Extent and terms of a thesis are specified in directions for its elaboration that are opened to the public on the web sites of the faculty.

Supervisor: **doc. Ing. Lenka Kulhánková, Ph.D.**

Date of issue: 26.10.2017

Date of submission: 21.05.2018

prof. Ing. Jaromír Pištora, CSc.
Head of Department

Ing. Zdeňka Chmelíková, Ph.D.
Vice-rectress for Study Affairs

VYSOKÁ ŠKOLA BÁŇSKÁ - TECHNICKÁ UNIVERZITA OSTRAVA
UNIVERZITNÍ STUDIJNÍ PROGRAMY

Prohlašuji, že jsem celou diplomovou práci včetně příloh vypracovala samostatně pod vedením vedoucího diplomové práce a uvedla jsem všechny použité podklady a literaturu. Byla jsem seznámena s tím, že na moji diplomovou práci se plně vztahuje zákon č. 121/2000 Sb. – autorský zákon, zejména §35 – užití díla v rámci občanských a náboženských obřadů, v rámci školních představení a užití díla školního a §60 – školní dílo. Beru na vědomí, že Vysoká škola báňská – Technická univerzita Ostrava (dále jen VŠB-TUO) má právo nevýdělečně ke své vnitřní potřebě diplomovou práci užít (§35 odst. 3). Souhlasím s tím, že jeden výtisk diplomové práce bude uložen v Ústřední knihovně VŠB-TUO k prezenčnímu nahlédnutí a jeden výtisk bude uložen u vedoucího diplomové práce. Souhlasím s tím, že údaje o diplomové práci, obsažené v Záznamu o závěrečné práci, umístěném v příloze mé diplomové práce, budou zveřejněny v informačním systému VŠB-TUO. Bylo sjednáno, že s VŠB-TUO, v případě zájmu z její strany, uzavřu licenční smlouvu s oprávněním užít dílo v rozsahu §12 odst. 4 autorského zákona. Bylo sjednáno, že užít své dílo – diplomovou práci nebo poskytnout licenci k jejímu využití mohu jen se souhlasem VŠB-TUO, která je oprávněna v takovém případě ode mne požadovat přiměřený příspěvek na úhradu nákladů, které byly VŠB-TUO na vytvoření díla vynaloženy (až do jejich skutečné výše). Beru na vědomí, že odevzdáním své práce souhlasím se zveřejněním své práce podle zákona č. 111/1998 Sb., o vysokých školách a o změně a doplnění dalších zákonů (zákon o vysokých školách), ve znění pozdějších předpisů, bez ohledu na výsledek její obhajoby.

Koníčková

V Ostravě: 21. 5. 2018 Hana Koníčková

K Vodárně 135, 742 83 Zbyslavice

Prohlašuji:

Prohlašuji, že svou diplomovou práci na téma: "Synthesis and characterization of polypyrrole layers on different substrates", jsem vypracovala samostatně s použitím doporučené literatury. Tímto dávám souhlas k jejímu dalšímu využití.

V Ostravě: 21. 5. 2018 Podpis:.....

Anotace

Tato práce se zaměřuje na přípravu a charakterizaci polypyrrolových vrstev na různých substrátech. Příprava polypyrrolových vrstev probíhala jednoduchou metodou za použití chloridu železitého jako oxidačního činidla na několika typech substrátu – sodnovápenatém skle, polyethylentereftalátové folie a křemíkové desce. U připravených vrstev byla změřena jejich vodivost a dále byly charakterizovány pomocí optického mikroskopu a Ramanovy spektroskopie. Vytvořením série modelů molekulárním modelováním a jejich následnou optimalizací bylo možné vypočíst a srovnat interakční energie polypyrrolových vrstev na použitých substrátech.

Klíčová slova: polypyrrol, vrstvy, molekulární modelování.

KONÍČKOVÁ, Hana. *Synthesis and characterization of polypyrrole layers on different substrates*. Ostrava, 2018. Diplomová práce. Vysoká škola báňská – Technická univerzita Ostrava. Vedoucí práce doc. Ing. Lenka Kulhánková, Ph.D., 54s.

Annotation

This work focuses on preparation and characterisation of polypyrrole layers on different substrates. The preparation of polypyrrole layers was carried out by a simple method using ferric chloride as an oxidising agent on several types of substrates - soda lime glass, polyethylene terephthalate foil, and the silicon wafer. The conductivity of the prepared layers was measured, they were then further characterised by an optical microscope, and Raman spectroscopy. By creating a series of models with molecular modeling and their subsequent optimisation, it was possible to calculate and compare the interaction energy of polypyrrole layers on the used substrates.

Keywords: polypyrrole, layers, molecular modeling.

KONÍČKOVÁ, Hana. *Synthesis and characterization of polypyrrole layers on different substrates*. Ostrava, 2018. Diploma thesis. VŠB – Technical University of Ostrava. Supervisor Assoc. Prof. Ing. Lenka Kulhánková, Ph.D., 54s

Content

Introduction

This thesis focuses on preparation, characterisation, and comparison of polypyrrole films on different substrates. The very first step of this work was a literature study of the layers´ preparation method to find the easiest and most efficient one. A simple method, which is described furtherly, was used to prepare samples with several amounts of polypyrrole. Conductivity was measured for the prepared samples, and they were also analysed with 3D optical microscopy and other instrumental techniques (Raman spectroscopy and Scanning electron microscopy). Subsequently, the Materials Studio software was used for building and further processing of atomistic models of prepared samples. The built atomistic models were used to calculate the adhesive energy of polypyrrole layers to individual substrates. Finally, the samples were compared according to their conductivities and interaction energies to determine the best samples.

1. Theoretical part

2.1 Conducting polymers

Polymers consist of repeated constitutional units (mers) and form long chains. Common polymers (for example polyethylene or polyvinylchloride) are not able to lead electric current and are used as electrically insulating materials. However, there exists a group of polymers which allows electricity to pass through it. Conducting polymers (e.g., polyaniline, polypyrrole or polyacetylene) have contrasted to the other polymers, their ability to lead electric current – their electrical conductivity. They are composed of a system of conjugated double bonds which, together with the presence of charge carriers, are preconditions for electrical conductivity [1].

The equally shared feature in the structure of conducting polymers is polyconjugation in the π-system of their backbone. The conducting polymers (also termed synthetic metals) are polyconjugated – which own electrical properties of metals while keeping the mechanical properties and processability of formal polymers. They achieve high conductivity because of incorporation of small concentrations of dopants into the matrix of the original polyconjugated polymers that have conductivity in the range from 10^{-10} to 10^{-5} $S \cdot cm^{-1}$. The end materials have conductivities from 1 to 10^{5} $S \cdot cm^{-1}$ that are typical for semiconductors or metals [2].

Nowadays, conducting polymers are renowned materials that have a wide variety of use [3].

2.1.1 Polypyrrole

Lately, conducting polymers have been studied as advanced materials. Among the numerous conducting polymer, polypyrrole (PPy) is by far the most extensively studied, which is due to its ease of synthesis, good redox properties, stability in the oxidized form, ability to give high electrical conductivity, commercial availability and useful electrical and optical properties [4]. Oligomer products were acquired by chemical oxidation of pyrrole in 1887. The fact that pyrrole polymerizes in acidic environment by oxidation with hydrogen peroxide to form an insoluble “pyrrole black” was published in 1916. Pratesi [6]shows the composition of PPy $C_{4.00–4.5}$ $H_{3.0–4.5}$ $N_{1.0}$

$O_{1.0–1.5}$. It is evident that the structure shown in Fig. 1 represents an ideal form of PPy, without the presence of oxygen [5].

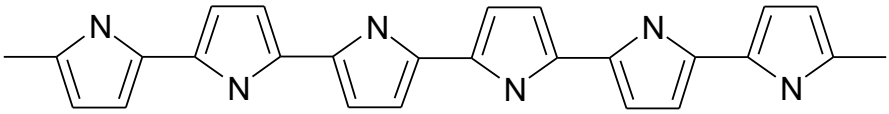

Fig. 1 *Polypyrrole chain.*

2.1.2 Properties of polypyrrole

Pyrrole black is a product of chemical oxidation of pyrrole. Many of PPy properties are studied on electrochemically prepared PPy thin films. Precursors (dopant, solvent – in electrochemical polymerisation) used for the preparation of PPy also have an impact on electrical conductivity [2]. The stability in the air is comparatively high. Therefore, their degradation occurs only above 150 – 300 °C (according to the dopant anion). The thermal analysis affirms that the PPy is thermally stable below 250°C and above this temperature, the rate of weight loss enhances and becomes very fast from above 600°C [6]. The thermal degradation of PPy begins with the decomposition or decrease of used dopant. Another deprotonation (or subsequent decrease of dopant) at higher temperatures always goes together with a formation of structures of imine shape in the polymer [2].

The PPy is without definite shape and commonly gives just a diffuse halo in X-ray diffraction patterns. The electron diffraction experimental data revealed that there are up to 15% (of the whole volume) of crystalline domains in the bulk of amorphous PPy and that the crystalline regions´ lattice is monoclinic. That means that nitrogens in pyrrole rings are oriented in opposite directions (Fig. 2) [2].

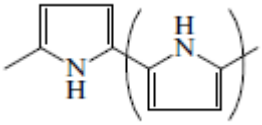

Fig. 2 *Orientation of pyrrole rings [2].*

The obtained data from nuclear magnetoresistance analysis and infrared spectroscopy of the products of oxidative decomposition of PPy demonstrate that pyrrole rings connect in α–α′ positions. This conclusion confirms by the fact that α–substituted pyrrole derivatives do not polymerise upon oxidation. The theoretical calculations indicate that a certain amount of bonds is formed in β – positions [2].

The PPy chains are planar, and they are arranged in layers parallel to the substrate surface (the distance between plains is 0.341 nm). The PPy chains in the plain are not oriented. The anions of the dopant fill in the interplanar space between the PPy chains. The electrostatic interactions between oxidised PPy chains and dopant anions happen through the π–system of the rings rather than through heteroatoms of the rings (shows the X-ray photoelectron spectroscopy). The electron diffraction´s data shows that in the film the polymer chains are order into layers. The fast charge transfer along the polymer chains and the rapid exchange between the macromolecules are related to studies of conductivity which also indicates that polymer chains are, to a certain amount, ordered. The degree of polymer ordering influences the PPy conductivity heavily. X-ray diffraction showed that a presence of multi-charged anions in the process of preparation of the PPy films has a different effect on the regularity of the film (films are more ordered) than a presence of single-charged anions [2].

PPy is insoluble in organic solvents which is a troublesome problem for the measurement of its molecular mass [2].

The mechanism of charge transport is a particular subject of interest in PPy conduction. The charge carriers are polarons and bipolarons, and doping forms them. From the chemical point of view, the formation of a polaron is the same to the creation of a radical cation (Fig. 3), and formation of a bipolaron is the same to the formation of a dication (Fig. 4) [2].

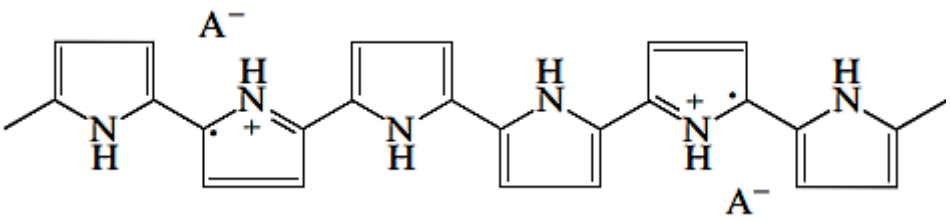

Fig. 3 *Polaron [2].*

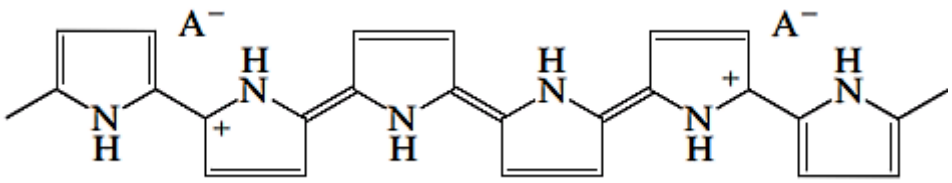

Fig. 4 *Bipolaron [2].*

The polaron and bipolaron are lengthened structures that spread over three to four monomer units of the chain. The calculations of the energies demonstrated that the formation of a bipolaron requires 0,45 eV less than the creation of two polarons [2]. The spectroelectrochemical measurements revealed that polarons in PPy are stable species and their maximum concentrations are between 80% and 90% [8]. Further investigation of PPy using in situ impedometry demonstrated that polarons and bipolarons equally contribute to conductivity, being charge carriers with the same mobility [9].

Particular interest is placed on interchain interactions and the charge transfer. The dopant, used in synthesis, compensates the charge of free charge carriers and also amplifies the probability of interchain charge transfer because of significant overlap of dopant's atomic orbitals with the π–orbitals of the atoms of carbon. The conductivity along the surface is for the most part higher than perpendicular because the polymer chains are primarily oriented parallel to the film surface. There also exist records that the conductivity increases with decreasing temperature (which is a behaviour intrinsic to metals). The conditions of polymers' synthesis massively affect their conductivity. Significant changes in conductivity usually appear in the earlier phases of doping, and its additional increase negligible [2].

The conductivity of PPy films can shift by several decimal orders and is dependent on the anion used in the synthesis. In most cases, the conductivity is higher for anions that share lower nucleophilicity. When stored in air, the PPy films start to lose their conductivity (the conductivity of the films with large organic anions is reducing more slowly) [2].

2.1.3 Synthesis of polypyrrole

The electrochemical way of preparation of PPy has been discovered after 1979 as a part of important development of conducting polymers. PPy has been prepared from monomer solution in acetonitrile or propylene carbonate with low water content in the presence of dopant (e.g. tetramethylammonium tetrafluoroborate). A film, which conductivity reached up to 100 $S \cdot cm^{-1}$, was created on platinum electrode [10]. Further study revealed that it is a polymer containing pyrrole cores connected in α and α´ positions to the polymer chain [6].

Papers that describe electrochemical synthesis of PPy in aqueous solutions have been published in 1982. Nevertheless, the mechanism of electrochemical polymerisation of pyrrole is not fully understood. A creation of pyrrole cation radical assumes to be the very first step. Afterwards, it reacts with another created cation radical to form a dimer while eliminating two protons. The propagation of the chain proceeds like a recombination of a dimer radical with other cation radicals for simultaneous deprotonation [6].

In comparison, chemical polymerization of pyrrole is more productive than electrochemical polymerization. In order to obtain higher amount of product with high conductivity, many laboratories are working on improving the process of chemical polymerization of pyrrole. Chemical way of preparation uses vide range of oxidizing agents – e.g. here used ferric chloride (preferred also in application for higher conductivity of prepared PPy) or other like ammonium peroxydisulfate, hydrogen peroxide, and different kind of salts containing ions of transition metals (e.g. Cu^{2+}, Cr^{6+}, Ce^{4+}, Fe^{+3}, Ru^{3+}, and Mn^{7+}) [6].

The Fig. 5 shows reaction scheme for the chemical polymerization of pyrrole. In the first steps (a, b), pyrrole is transformed into its radical cation after oxidation and then two such radicals form a pyrrole dimer (c). Pyrrole dimer is then oxidized again to form a pyrrole dimer cation (d). Lastly, large number of pyrrole dimer cations interact with radical cations to form the polymer chain of PPy (e) [11].

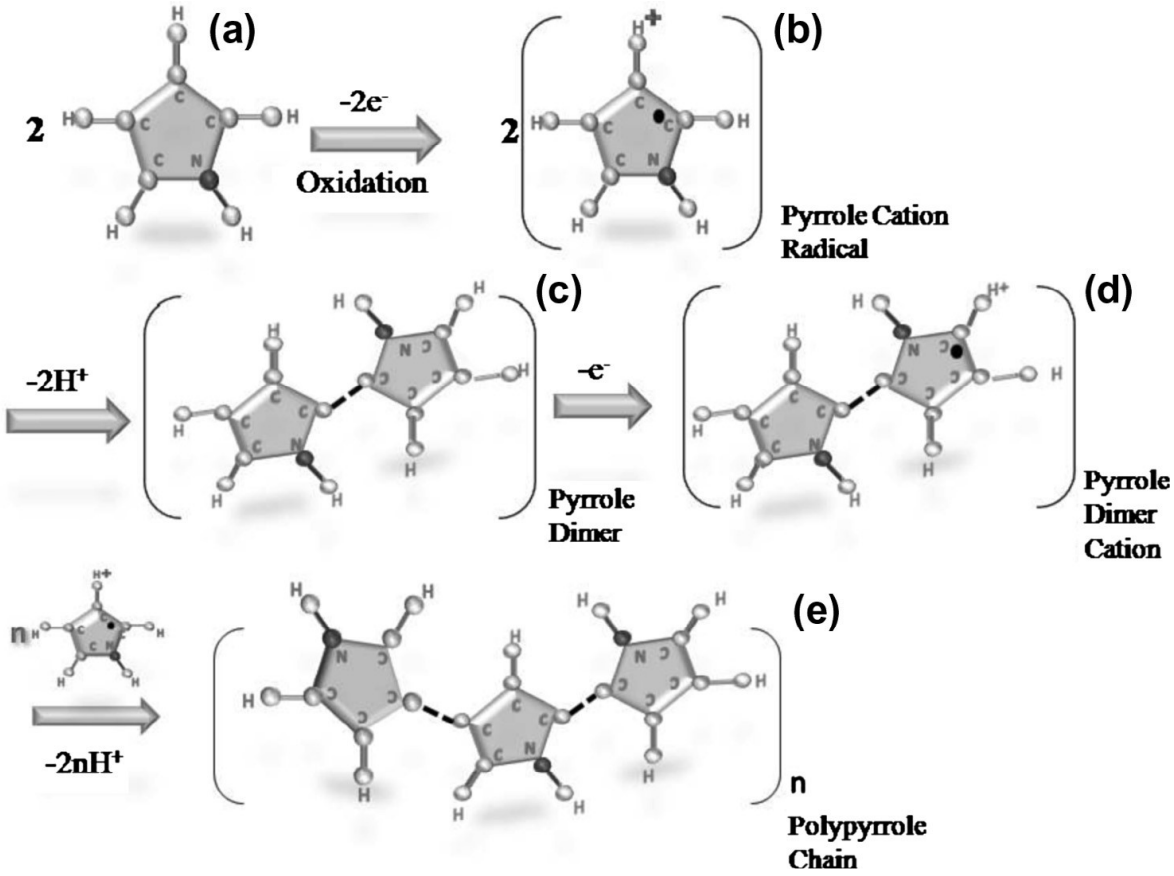

Fig. 5 *The reaction mechanism of chemical polymerization of pyrrole [11].*

Thin films of PPy are preferably deposited on hydrophobic surfaces from diluted aqueous solutions of the polymerizing monomer [12].

2.1.4 Utilization of polypyrrole thin films

According to first electrochemical studies, PPy thin films can be, thanks to their great stability, used like non-metal electrodes [2]. Its biocompatibility together with great stability provides a great environment for growing nerve tissues. The doping anion in polypyrrole plays a key role in determining the physical and chemical properties of this conductive polymer. Other properties of the doping anion include the ability to incorporate and release the neurotrophin protein - neurotrophin-3. The multidimensional role of the dopant is critical for ensuring optimal performance of polypyrrole when used as a platform for nerve growth. The effect on compatibility of the dopant used in the electrochemical synthesis of polypyrrole with the primary auditory nerve tissue is considered and compared to some of the physical properties of the films. Significant differences in the controlled release properties of the films were

also observed. The ability of polymers to increase nerve growth and their survival in vitro with the release of neurotrophin-3 (NT-3) is a function of both nerve tissue compatibility and the ability of the polymer to release sufficient neurotrophic protein to affect cell growth. Para-toluenesulfonate (pTS) is a small synthetic dopant that works favourably in both aspects and has proven to be the most suitable material for neurotrophin transport for inner ear therapy [13].

Preparation of electrically conducting material is also key aspect of nerve tissue engineering. In this case, by the process of chemical oxidation, emulsion polymerization, was prepared the highly conductive polypyrrole/graphene nanocomposite (PYG), which was used to produce new conductive porous scaffolds based on gelatin/chitosan matrix. An examination of the different properties of scaffolding was carried out, depending on the PYG content. Tests revealed significant biocompatibility of Schwann cells and a low PYG. The composite of gelatin/chitosan/PYG has potential to be used in nerve tissue engineering for applications which electrical stimulation plays an important role [14].

Another usage of the PPy film is covering semiconductor. It prevents passivation of its surface and at the same time allows the formation of the electron holes, which pass to the polymer (PPy film stabilizes semiconductor surface against degradation while permitting electron exchange with the electrolyte). Such systems were studied for example for GaAs anodes. It was demonstrated that such polymer films prevent photodegradation of the semiconductor, probably by impeding ion/solvent transport. The short-circuit photocurrent for the bare (unprotected) semiconductor drops very quickly (within a few minutes), probably because of formation of an insoluble blocking surface layer of photodecomposition product, while for PPy-coated photoanodes stays basically the same. The PPy coating also affords n-GaAs electrodes protection from dissolution in aqueous electrolytes although in this case, stabilization is less obvious. If the surface is roughened before the film deposition it appears to improve adhesion [15].

During the last two decades, attempts had been made to manufacture junction devices using conducting polymers as an active material, which can replace the conventional anorganic semiconductors in the fabrication of photosensitive junctions in electronic and optical devices, such as solar cells. From this point of view, conducting polymer thin films have received big interest in many application fields because of their

chemical, physical, and mechanical properties. It has the characteristics of high sensitivities, short response times, and optimum performance at room temperatures. Since low-cost and easy manufacturing methods need to be employed for the fabrication of solar cell devices, PPy is suitable for its rather easy preparation, where pyrrole monomer is easily oxidized [16].

2.2 Molecular modeling

Molecular modeling serves as an efficient and effective tool for designing new functional nanostructures - nanomaterials with the required properties (allowing control of properties). It assumes the relationship between structure and properties of nanomaterials. The prediction of structure and properties saves material and energy to technologists. The energy of the system (molecules) can be imagined as a potential area where each shape of the molecule corresponds to the energy at that point. The molecular modeling method uses the calculation of the most stable configurations based on energy optimization of structures - the search for the minimum on the potential area of energies. In principle, we can divide it into molecular mechanics, molecular dynamics and classical molecular dynamics. Molecular mechanics optimizes structure and bond geometry by minimizing potential energy described by empirical force fields. In this case, kinetic energy equals zero. On the other hand, molecular dynamics utilizes the kinetic energy in the system and, depending on time, allows to study dynamic processes. In this thesis, molecular mechanics was used.

Chemists see molecules from the perspective of bond angles, bond lengths and dihedral angles. All this info is also included in the series of Cartesian coordinates for the constituent atoms (molecule containing N atoms has 3N Cartesian coordinates). Scientists who deal with spectroscopy are overall interested in finding a group of equilibrium, geometric parameters, and force constants that corresponds perfectly with their experimental data. They want a *force field* (containing force constants, equilibrium quantities, and every other comprised parameter) that is specific for a given molecule. They want their incredibly accurate measurements to agree with theory. If the force field contains only chemical terms (like bond lengths, bond angles and dihedral angles) it is denoted as a *valence force field*. Molecular modelers want a force field that can be transferred from molecule to molecule (for example to predict

the geometry of a new molecule using data they get from other kindred molecules). They make use of the bond concept referring to traditional ideas that a molecule is a number of bonded atoms and a large molecule consists of the same properties as small molecules but combined in different ways [17].

Empirical force fields are used for description of the potential energy of a system in molecular mechanics. It is a complex of empirical parameters which characterise bonding energy of two, three resp. four atoms. Those parameters are bond lengths, bond angles, torsion angels and nonbonding interactions.

Parameters and functional forms are the essential infrastructures of molecular mechanics and dynamics force fields. Unfortunately, the popular force fields, based on the classic work in the field, are limited to particular combinations of atoms, for example, those of proteins, organics, or nucleic acids [18].

In order to assist the progress of studies of a variety of atomic associations, a new force field has been developed using general rules for estimating force field parameters based on simple relations. This set of fundamental parameters depends only on the element, its hybridization, and connectivity. This new force field is declared as a Universal force field (UFF) [18].

The angular distortion functional forms in UFF are chosen to be physically reasonable for large amplitude displacements. The parameters worked with to generate the UFF involve a set of hybridization dependent atomic bond radii, van der Waals parameters, a set of hybridization angles, torsional and inversion barriers, and a set of effective nuclear charges. The elements in the UFF periodic table are the atom types. Atoms of the same type may only be similar physically and chemically, yet, as the norm says, they are treated alike in the force field. The UFF has 126 atom types [18].

The potential energy of an arbitrary geometry for a molecule is written as a superposition of various two-body, three-body, and four-body interactions. The potential energy is signified as a sum of valence or bonded interactions and nonbonded interactions:

$$E = E_R + E_\theta + E_\phi + E_\omega + E_{vdw} + E_{el} \quad (1)$$

E_R – bond stretching, E_θ – bond angle bending, E_ϕ – angle torsion, E_ω – inversion terms, E_{vdw} – van der Waals terms [18].

The valence interactions consist of bond stretching and angular distortions (bond angle bending, dihedral angle torsion, and inversion terms). The nonbonded interactions consist of van der Waals and electrostatic terms. The UFF describes the bond stretch interaction as either a harmonic oscillator:

$$E_R = \frac{1}{2} k_{IJ} \left(r - r_{IJ}\right)^2 \tag{2}$$

or as the Morse function:

$$E_R = D_{IJ} \left[e^{-\alpha (r - r_{IJ})} - 1\right]^2 \tag{3}$$

Where k_{IJ} is the force constant in units of (kcal/mol)/Å^2, r_{IJ} is the standard or natural bond length in Å, D_{IJ} is the bond dissociation energy (kcal/mol), and α is:

$$\alpha = \left[k_{IJ} \Big/ 2D_{IJ} \right]^{1/2} \tag{4}$$

The Morse function is a more precise description since it implicitly includes anharmonic terms near equilibrium (r_{IJ}) and leads to finite energy (D_{IJ}) for breaking bonds [18].

The natural bond length r_{IJ} (with parameters for a harmonic form of the bond stretch) is presumed to be the sum of atom type specific single bond radii, a bond order correction, and an electronegativity correction:

$$r_{IJ} = r_I + r_J + r_{BO} + r_{EN} \tag{5}$$

r_I, r_J – single bond radii, I, J – atom centres [18].

General Fourier expansions are employed in the UFF to describe all angular distortions because the expansions can be constructed: (a) to have derivatives that are singularity free, (b) to have the corresponding distortions for the large amplitude motions found in molecular dynamics simulations, and (c) so that the C_n coefficients can be simply chosen to satisfy suitable, physically justified, boundary conditions [18].

$$E_\gamma = K \sum_{n=0}^{m} C_n \cos n\gamma \tag{6}$$

In UFF, the angle bend term is described with a small cosine Fourier expansion in θ:

$$E_\theta = K_{IJK} \sum_{n=0}^{m} C_n \cos n\theta, \qquad K_{IJK} = \left(\frac{\partial^2 E}{\partial \theta^2}\right)_0 \tag{7), (8}$$

K_{IJK} – angle bend force constant, C_n – coefficient, θ – bending angle [18].

where the coefficients C_n, are chosen to satisfy suitable boundary conditions including that the function has a minimum at the natural bond angle θ_0. The torsional terms for two bonds IJ and KL connected via a common bond JK is described with a small cosine Fourier expansion in ϕ:

$$E_\phi = K_{IJKL} \sum_{n=0}^{m} C_n \cos n\phi_{IJKL} \tag{9}$$

where K_{IJKL} and the coefficients C_n, are determined by the rotational barrier V_ϕ, the periodicity of the potential, and the equilibrium angle. For UFF, a one- or two-term cosine Fourier expansion in ω is used for atoms I bonded precisely to three other atoms J, K, L:

$$E_\omega = K_{IJKL}\left(C_0 + C_1 \cos \omega_{IJKL} + C_2 \cos 2\omega_{IJKL}\right) \tag{10}$$

where K_{IJKL} is the force constant in (kcal/mol), and ω_{IJKL} is the angle between the IL axis and the IJK plane. Nonbonded interactions (van der Waals forces) are included in the Universal force field. A Lennard-Jones potential expression is used:

$$E_{vdw} = D_{IJ}\left\{-2\left[\frac{x_{IJ}}{x}\right]^6 + \left[\frac{x_{IJ}}{x}\right]^{12}\right\} \tag{11}$$

where D_{IJ} is the well depth in kcal/mol and x_{IJ} is the van der Waals bond length in Å. The valence parameters discussed in the above sections were obtained without partial charges. When included, electrostatic interactions are calculated by:

$$E_{el} = 322{,}0637\left(\frac{Q_i Q_j}{\varepsilon R_{ij}}\right) \tag{12}$$

Q_i and Q_j are charges in electron units, R_{ij} is the distance in Å, and ε is the dielectric constant. The default dielectric constant is 1 for UFF, and no distance cutoff is used. The partial charges are obtained using QEq charge equilibration. With UFF the usual convention of excluding van der Waals and electrostatic interactions for atoms that are bonded to each other or bonded to a common atom [18].

UFF is force field constructed from simple rules and atomic parameters and is capable of reproducing most structural features across the periodic table with errors less than 0.1 Å in bond distances and 5° to 10° in angle bend [18].

Molecular mechanics tends to be concerned about the search for minimum on the molecular potential energy plain of large molecules. This problem is denoted as an *optimization theory*. The first manual calculations for the molecular mechanics optimization were made by F. H. Westheimer in 1956. J. B. Hendrickson was later the first one, who has done the computer calculations. Unfortunately, their methods were not appropriate and applicable for molecules. Over the years, many algorithms have been developed (some of them suitable for molecular mechanics, some for quantum mechanics). The molecular mechanics must deal with large molecules whose molecular potential energy is dependent on hundreds or thousands of variables. On the other hand, assessment of the potential energy at each point on the hypersurface is comparatively quite easy. Optimization methods can be divided by the fact if they use or do not use derivatives. Methods using derivatives can be also divided into *first–order* derivative methods (they use gradient) and *second–order* derivative method (use both gradient and Hessian). From many algorithms only three will be described and are used in geometry optimization in this thesis. All three algorithms described below are part of a cascade of methods called "Smart" algorithm and are iterative. The Smart algorithm consist of Steepest descent algorithm, algorithm of conjugated gradients, and Quasi-Newton algorithm. Iterative algorithms start at initial point and then they move on in cycles (in accordance with the algorithm) to the stationary point. Each one of the cycles is called an iteration [17].

The first method is a first–order method Steepest descent. This optimization algorithm is the easiest one. It is commonly used on the start of the optimization process when the starting point is far away from the minimum of the potential energy plane. The method starts from a point on a potential energy surface and each and every step recognizes the direction of the greatest change of the potential plane (in the direction of the greatest negative gradient). Every next step has to be only perpendicular to the previous step. This forces every other step to make a right–angle turn at every point even it is not the best way to the minimum. This can also make the algorithm oscillating in flat areas on potential energy plain. The algorithm continues until a value of the gradient falls under the pre-set value of convergence criterium [17].

The second method also belongs to the first–order methods. It is an algorithm of conjugated gradients. It is similar as the Steepest descent algorithm but beside it uses all previous gradients and not only the one in the specific point, and subsequent gradients do not need to be perpendicular to each other – this enables faster and narrower path to the minimum. Conjugated here are not gradients but directions (more appropriate name would be algorithm of conjugated directions). It means that direction in next step does not interrupt the minimum from previous step. Output of this method is a set of directions that surpass the oscillatory behaviour of Steepest descent algorithm in flat area therefore it is placed after it in the cascade [17].

The third and last method is a Quasi–Newton algorithm and is included in second–order methods. This method is used when computing Hessian in iteration step is not possible or too hard to compute. In Quasi–Newton the Hessian matrix does not need to be computed and is replaced by its approximation. The approximation can be computed by various methods e.g. DFP (or Davidon, 1959, and Fletcher and Powell, 1963) or BFGS (for Broyden, 1969, Fletcher, 1970, Goldfarb, 1970, and Shanno, 1970). The BFGS is generally considered as the best performing method. The Hessian is updated by analysis of successive gradient vectors instead. It restricts the solution by adding an insignificant update to the current estimate of the Hessian [19].

A Gasteiger method was used for calculation of atomic charges of PPy chains. It is a rapid calculation of atomic charges in organic molecules with σ–bonded and nonconjugated π–systems. The good approximation, it suffices to consider the identity of the individual atoms and their connectivity to reproduce the charge distributions in molecules. The calculation only considers the connectivity of the atoms because they are characterized by their orbital electronegativities. Therefore, only the topology of a molecule is important. A partial equalization of orbital electronegativity is obtained through an iterative process. Thus, the topology of a molecule determines the nature of the electron distribution [20].

The Gasteiger method is not suitable for calculation of atomic charges of used substrates so, in this case a charge equilibration method (QEq) was used. Knowledge of the charge distribution within molecules is essential for determining the electrostatic energies (including hydrogen bonding) in molecular mechanics and molecular dynamics calculations. The charge equilibration (QEq) approach allows the charges to respond to changes in the environment, including those in applied fields, and can be

applied to any material (polymer, ceramic, semiconductor, biological, metallic). It is a great way how to predict charges of large molecules based only on geometry and experimental atomic properties [21].

In order to estimate the equilibrium charges in a molecule, first needs to be considered how the energy of an isolated atom changes as a function of charge. Using a neutral reference point, the energy of a single atom A can be written using Taylor´s polynomial (including only terms through second order) as:

$$E_A(Q) = E_{A0} + Q_A\left(\frac{\partial E}{\partial Q}\right)_{A0} + 1/2Q_A^2\left(\frac{\partial^2 E}{\partial Q^2}\right)_{A0} \tag{13}$$

where $E_A(0) = E_{A0}$ and Q_A is charge of the atom A. Energy for atom with charge Q= (+1) is then expressed as:

$$E_A(+1) = E_{A0} + \left(\frac{\partial E}{\partial Q}\right)_{A0} + 1/2\left(\frac{\partial^2 E}{\partial Q^2}\right)_{A0} \tag{14}$$

and energy for atom with charge Q= (-1) as:

$$E_A(-1) = E_{A0} - \left(\frac{\partial E}{\partial Q}\right)_{A0} + 1/2\left(\frac{\partial^2 E}{\partial Q^2}\right)_{A0} \tag{15}$$

Chemical potential of the single atom A is then determined from a difference of equations for Q= (±1) like:

$$\chi_A^0 = \left(\frac{\partial E}{\partial Q}\right)_{A0} = \frac{IP+EA}{2} \tag{16}$$

where IP and EA are the ionization potential and electron affinity defined as:

$$IP = E_A(+1) - E_{A0},\ EA = E_A(-1) - E_{A0} \tag{17}$$

From the sum of the equations for Q= (±1) then we get the formula for repulsion of electrons in an orbital:

$$J_{AA}^0 = \left(\frac{\partial^2 E}{\partial Q}\right)_{A0} = IP - EA \tag{18}$$

After fitting chemical potential and repulsion into formula for energy of a single atom we get equation:

$$E_A(Q) = E_{A0} + \chi_A^0 Q_A + 1/2J_{AA}^0 Q_A^2 \tag{19}$$

When we consider two (or more) atomic systems, in the repulsion summation needs to be taken into account also a distance between the atoms:

$$J_{AA}^{0} = \frac{14{,}4}{R_A^0} \tag{20}$$

where 14,4 is a value of a conversion factor that allows $R_A^0$to be in Å and J_{AA}^{0} to be in eV. The equation for multiatomic system then is:

$$E(Q_1, \dots Q_N) = \sum_{A=1}^{N}(E_{A0} + Q_A\chi_A^0) + \frac{1}{2}\sum_{A=1}^{N}\sum_{B=1}^{N}(Q_A Q_B J_{AB}) \tag{21}$$

The QEq method uses only effortlessly available experimental data (atomic radius, atomic IP, and atomic EA) and for that reason can be applied to any combination of atoms [21].

2. Practical part

3.1 Preparation of polypyrrole thin films

3.1.1 Used materials

All used chemicals – pyrrole, ferric chloride and methanol – were purchased from Lach–Ner, Czech Republic. Microscope slides, made from soda lime glass with dimensions 26mm×26mm×1mm, purchased from Paul Marienfeld GmbH & Co. KG, Germany, were used as a glass substrate. Polyethylene terephthalate (PET) foil was purchased from RAYFILM s.r.o., the Czech Republic. Silicon wafers (100) were obtained from ON Semiconductor Czech Republic, s.r.o.

3.1.2 Method of synthesis

PPy layers were prepared by oxidative polymerization of the solution of pyrrole by ferric chloride. This process was selected as the easiest one from various processes that were studied in a literature review [3], [11], [22]-[26]. It does not need any special equipment, and the preparation is carried out at room temperature. The water solution of the monomer (pyrrole) was prepared in three different concentrations 0.15; 0.4; and 0.8 M. The water solution of the oxidizing agent ($FeCl_3$) had 0.2 M concentration. Before the polymerizations, substrates were cleaned with soap and then rinsed with distilled water and ethanol. Afterwards, they were taped with an adhesive tape from the bottom to secure the growth of a layer on only one side. They were then placed into the Petri dish (or beaker) by taped side facing the bottom leaving an additional strip of adhesive tape secured to the side of the dish for easier pulling out. The solution of monomer was dropping into the petri dish filled with the solution of oxidizing agent, and the substrate on the bottom (drops did not fell directly on the substrate – only near it). Time of the dropping was 2 hours, and after that, the solution stood still for 30 minutes. The substrate was then taken out and rinsed with distilled water and methanol. Lastly, it was dried by flowing air to speed up the drying process. The polymerization process starts immediately after the start of the drip. The water solution of the oxidizing agent ($FeCl_3$) turns from colorless to black within the period of time. It is though interesting that after all monomer in the solution is consumed in the polymerization process, the solution is then clear again and all product sticks to

beakers walls and bottom (there is also formed a thin crust on the surface of the solution).

Furthermore, the preparation process with the same input components was tried, but with different placement of the glass substrate. While was the glass substrate was hung up, the resulted layers have not created homogeneous cover of the substrate. Further, the substrate was placed by taped side up, and hung in the middle of the oxidant solution horizontally with the bottom. Thus, layers appeared homogeneous, were transparent but did not conduct (B series of prepared samples).

The other prepared layers were hung in the beaker by the taped side facing the bottom, and the solution was stirred to the lowest possible degree. Both the dropping and polymerization time were only 30 minutes (60 minutes total) and monomer and oxidant solutions were doubled (60 ml) while maintaining concentrations (0.2 M $FeCl_3$, 0.15 / 0.4 / 0.8 M Pyrrol). The layers were removed from the solution and washed with distilled water and methanol, followed by drying. The resulting layers were not homogeneous, and even at the lowest possible degree of stirring, the vortex was visible on the layers.

Additionally, layers with a combination of ammonium peroxodisulfate (APS) and $FeCl_3$ as an oxidizing agent (0.01 M APS + 0.01 M FeCl3 solution) were prepared. The monomer solution also had a concentration of 0.01 M. The APS and $FeCl_3$ solutions were mixed in the beaker (25 mL + 25 mL) and stirred for 15 minutes. The glass was hung in the beaker, taped with adhesive tape on one side. A solution of the monomer (50 ml of 0.01M) was added dropwise - in the original procedure, add until the solution turns black - even after adding 50 ml of the monomer solution, the solution was completely black. A "black border" appeared at the bottom of the beaker, but it did not blacken the entire volume. After 30 minutes, the slides were removed and washed twice with distilled water. No layer was created.

The Modification of the 1. successful preparation process (described above) by changing the oxidizing agent for APS did not lead to anything meaningful. The layers were washed from the slides by washing with water and methanol in final steps.

Prepared samples and used materials for each sample are summarized in **Table 1**.

Samples were denoted as

N_X_S,

Where **N** is letter differing the samples by the order of preparation, **X** stands for the concentration of the pyrrole solution used in sample preparation, and **S** means the type of used substrate (e.g., G is glass, PET is polyethylene terephthalate foil, and Si is silicon wafer). In the beginning, I wanted to name the samples by the day of preparation but that would mean an unnecessarily long name for further analysis, so I denoted the samples according to the used substrate with the information of the order of preparation hidden in the first letter of the sample's name.

Table 1 *List of prepared samples and used materials for each sample.*

Sample	C_{PPy} [mol/dm^3]	V_{PPy} [dm^3]	Oxidizing agent	C_{FeCl3} [mol/dm^3]	V_{FeCl3} [dm^3]	Substrate
A_0,15_G	0,15	0,03	$FeCl_3$	0,2	0,03	glass
A_0,4_G	0,4	0,03	$FeCl_3$	0,2	0,03	glass
A_0,8_G	0,8	0,03	$FeCl_3$	0,2	0,03	glass
B_0,15_G	0,15	0,03	$FeCl_3$	0,2	0,03	glass
B_0,4_G	0,4	0,03	$FeCl_3$	0,2	0,03	glass
B_0,8_G	0,8	0,03	$FeCl_3$	0,2	0,03	glass
C_0,15_G	0,15	0,03	$FeCl_3$	0,2	0,03	glass
C_0,4_G	0,4	0,03	$FeCl_3$	0,2	0,03	glass
C_0,8_G	0,8	0,03	$FeCl_3$	0,2	0,03	glass
D_0,15_PET	0,15	0,03	$FeCl_3$	0,2	0,03	PET foil
D_0,4_PET	0,4	0,03	$FeCl_3$	0,2	0,03	PET foil
D_0,8_PET	0,8	0,03	$FeCl_3$	0,2	0,03	PET foil
E_0,15_Si	0,15	0,03	FeCl3	0,2	0,03	Si wafer
E_0,4_Si	0,4	0,03	FeCl3	0,2	0,03	Si wafer
E_0,8_Si	0,8	0,03	FeCl3	0,2	0,03	Si wafer

Fig. 6 The picture of the sample E_0,8_Si.

In the Fig. 6 there is a photo of prepared layer on Si wafer substrate. All prepared layers looked alike. They were black, homogenous and uniform.

3.2 Analysis of prepared samples

The conductivity measurements were performed for prepared samples. After that the samples were analysed with optical microscope and Raman spectroscopy. The interaction energy was also compared within substrates by molecular modeling.

Conductivity measurement: The conductivity of prepared samples was obtained by an indirect method (subsequent calculation) from the measurement of a currnet of the samples. The instrumentation for measurement consists of 2 flat electrodes (3 mm apart) connected to the source, the data collected from the electrodes were subsequently digitally transferred to the computer. The measurement was carried out in period of 300 s with the voltage set to 1V. The conductivity was then calculated from an average value of measured current.

Optical microscopy: Measurement was performed on Digital microscope VHX (Keyence Corporation, Japan). A scratch was made on the sample (through the layer to the substrate) where a surface image was taken at various magnifications, though it showed that 1000 times magnification was most clear in layers´ description. Also, a 3D image of the surface was created by a 3D measurement of the surface by the microscope. This 3D image was further processed in the *Gwiddyon* software where it

was possible to obtain the average thickness of the preparade layer by interleaving the 3D surface image by curves.

Raman spectroscopy: Raman spectra were collected on Smart System XploRA™ (Horiba Jobin Yvon, France) using 532 nm laser source. An Olympus microscope BX 41/51 with an objective magnification of 100 was used to focus the laser beam on the sample placed on an X–Y motorized sample stage. The filter was used to reduce laser beam to 1% of the initial laser beam (in case of foils and glass substrate), and 10% (in case of silicon wafer substrate) and grating 1800 grooves/mm were used. Acquisition time was set to the 30 s. All discussed spectra were calculated as average spectra from measurements in different points in each sample.

Molecular modeling: Models were prepared in BIOVIA Materials studio v0.7. I prepared series of atomistic models for each type of substrate differing by a number of PPy chains, their position on the substrate, and their tilt. All prepared models were built with polaron chains of PPy (charge 2+ per 10 mers) and adequate amount of Cl- ions to compensate the charge of PPy chains. Charges for PPy chains, and PET substrate were calculated by Gasteiger method [20]. Charges for Silicon structure, and a glass substrate were calculated by QEq approach [21]. Silicon substrate was built from the imported structure of pure Si from the library of Materials Studio software. PET substrate was built according to it crystal structure by knowing the position of each atom in the basic cell [27]. However, building a model of the glass substrate was a little more complicated. First, an analysis of the glass slide was made to know exact compounds of the glass. This revealed that it is made of soda lime glass that contains sodium and calcium ions. I found a creation process of model of such type of glass and followed its´ steps [28]. First, I needed to accommodate used dimensions of the cell to be able to contain the PPy chains and to maintain density described in the process I followed. After creating a cell of proper parameters containing an appropriate quantity of atoms, the modelled structure was subjected to simulated annealing (NVT, Universal force field [18], initial temperature 300 K, mid-cycle temperature 6000 K, 2 or 6 anneal cycles). Afterwards, the atoms in the selected model (according to the lowest total potential energy) were optimized in module Forcite (Universal force field [18], smart algorithm). The bonds were then added to this model and it was again optimized under the same conditions. Then the optimized structure was cleaved into the surface along (0 0 1) plane. All prepared substrates were built with 30 nm high vacuum slab. For each substrate, the models contained 1, 3 or 4 PPy chains. After

preparatiom, the models were optimized in Forcite module (Universal force field [18], smart algorithm), the maximum amount of iterations was set to $5 \cdot 10^5$ and pressure was set to 101 325 Pa. The calculation was done when potential energy has reached the accuracy of 0.001 kcal/mol and the force reached an accuracy of 0.5 kcal/mol/Å. For each substrate, energies were summarized and compared in order to reveal how does the position of PPy chains on the substrate affects the interaction energy.

3.3 Results

3.3.1 Results of analysis

Conductivity measurement: Following table () contains average values of conductivity σ calculated from the formula:

$$\sigma = \frac{lG}{S}, G = \frac{1}{R} = \frac{I}{U}$$

Where l is distance between electrodes in m, S is the cross-sectional area of the conductor (here defined by the length of the electrode, and layer's thickness) in m^2, G is electrical conductivity defined as an inverted value of a resistance, I is current in A, and U is voltage in V. After fitting, the formula for σ is:

$$\sigma = \frac{l \cdot I}{S \cdot U}$$

The conductivity unit is S/m [29]. Table 2 gives an overview of prepared samples, their calculated conductivities, measured average values of current, and thickness of prepared layers.

Table 2 *List of calculated and measured values of conductivity, current and layer thickness for all prepared samples.*

Name of sample	Conductivity [S/m]	Average current [μA]	Layer thickness [μm]	Average deviation for layer thickness
A_0,15_G	2,54	1678,52	79,32	8,76
A_0,4_G	9,41	9609,32	122,58	10,01
A_0,8_G	10,67	17147,98	192,88	40,71

B_0,15_G	-	-	-	-
B_0,4_G	-	-	-	-
B_0,8_G	-	-	-	-
C_0,15_G	2,72	2617,31	115,28	65,50
C_0,4_G	5,03	9032,12	215,43	7,07
C_0,8_G	1,04	2983,39	343,65	30,05
D_0,15_PET	0,62	179,76	34,72	14,30
D_0,4_PET	1,84	1363,84	89,19	24,97
D_0,8_PET	1,15	992,67	103,75	15,55
E_0,15_Si	2,21	1415,23	76,83	6,17
E_0,4_Si	7,67	6997,84	109,52	27,59
E_0,8_Si	10,79	14235,72	158,33	12,22

If we look at the prepared layers from the point of view of conductivity, we can say with certainty that PET substrate is the worst one and Si, and glass substrates are on the same level. The conductivity measured on Si substrate shows increasing trend in comparison with other substrates, however, this trend occurred on the first samples (A) prepared on the glass substrate but it was not confirmed on the third prepared samples (C) which were prepared as controlling samples to confirm the correctness of the preparation process. This deviation can be caused by different conditions (temperature, humidity) of preparation in the laboratory, because the samples were prepared in another part of year which could influence the temperature in the lab. Second prepared samples (B) on glass had a different position of the substrate in the petri dish. The glass was hung up in the petri dish by the taped side facing up. In the performed conductivity measurement, this sample did not conduct at all. From the point of view of layer thickness, the Si and glass substrates have similar values in comparison with PET foil, which has the lowest values for layer thickness.

Optical microscopy: Optical microscope analysis gives an interesting closer look at the structure of the prepared PPy layers. Even if layers look smooth for the first sight, from the closer look can be said that they consist of two sublayers that can be distinguished as a glossy wrinkled layer (occurring in all prepared samples) covered with dendritic PPy (which does not occur in non-conductive layers). The fact that dendritic PPy is not on the non-conductive layers leads me to the conclusion that it is worth conductivity of the other prepared layers. In following figures (Fig. 7 – Fig. 16) are compared presented microscope pictures of all prepared samples.

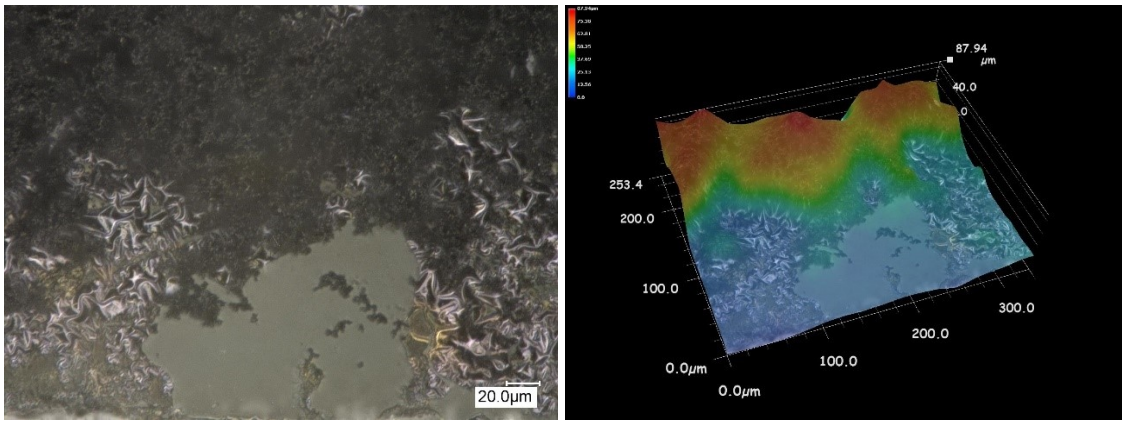

Fig. 7 *Picture of the surface of the sample A_0,15_G; the 3D image of the sample´s surface.*

In Fig. 7 on the left, there is measured the surface of the sample A_0,15_G measured at 1000 times magnification (1000x). There is visible glossy wrinkled layer lying directly on the glass substrate. On the wrinkled layer is then visible dendritic PPy. On the right, there is a 3D map of the surface.

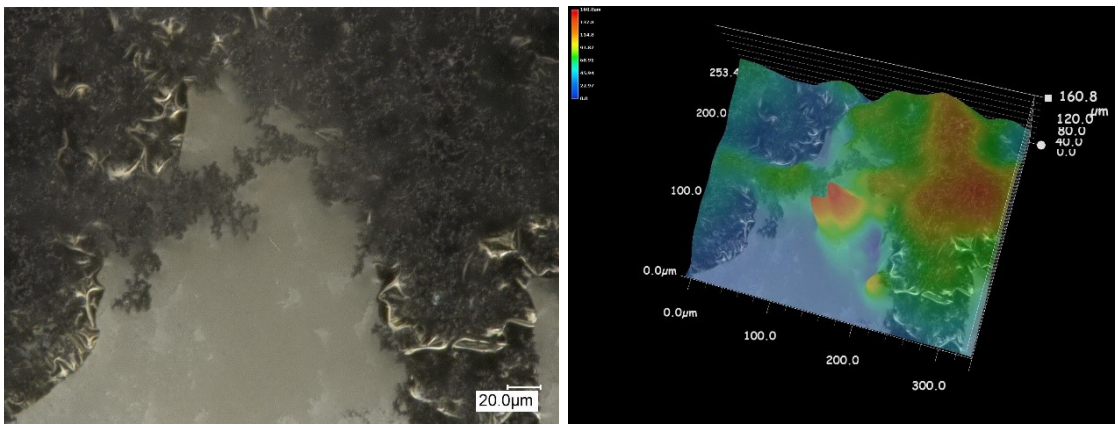

Fig. 8 *Picture of the surface of the sample A_0,4_G; the 3D image of the sample´s surface.*

In the Fig. 8, the dendritic PPy can be seen to form tufts (clumps), while the glossy wrinkled layer forms a uniform surface that is disturbed by the scratch created for measurement. Also measured at 1000x magnification.

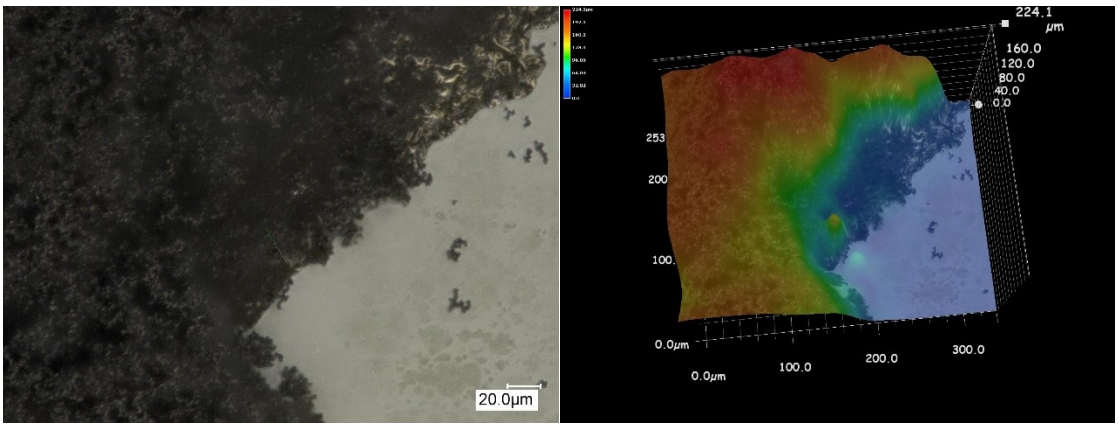

Fig. 9 *Picture of the surface of the sample A_0,8_G (left); the 3D image of the sample´s surface (right).*

On the sample with the highest concentration of Py solution (A_0,8_G), there is a much larger amount of dendritic PPy than on the sample with the lowest concentration of Py (A_0,15_G). Here, the dendritic PPy essentially completely covers the glossy wrinkled layer, which is only visible at the point where the dendritic PPy was wiped off the glossy wrinkled layer during formation of the scratch (Fig. 9).

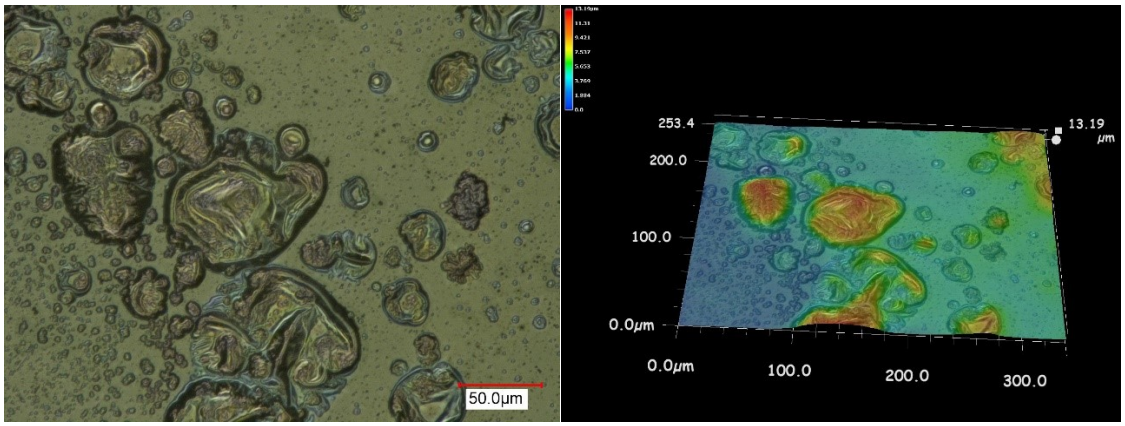

Fig. 10 *Image of the sample´s surface (left), and 3D surface´s image (right) of sample B_0,15_G.*

At a low Py concentration, the wrinkled layer in non-conducting samples was not formed uniformly, but in the form of bubbles (Fig. 10). From the 3D image of the surface, after comparison with the first prepared samples (A series), it is obvious that the layer has only a fraction of the thickness of the conductive samples. Again, 1000x magnification was used.

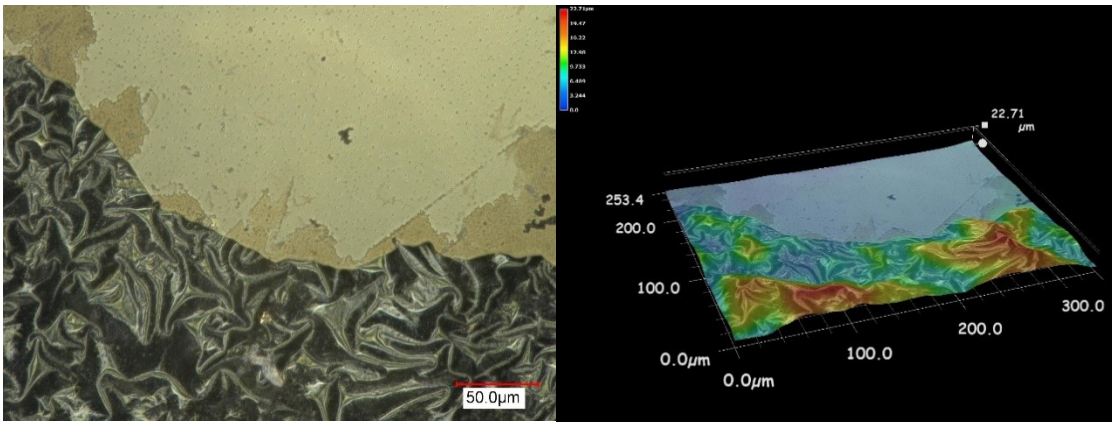

Fig. 11 *Image of the sample´s surface (left), and 3D surface´s image (right) of sample B_0,4_G.*

Increasing concentration of Py solution resulted in the formation of a uniform glossy wrinkled PPy layer on the glass surface (Fig. 11). There is none dendritic PPy, visible on B series of samples, which occurs at all other samples series. The measurement was performed at 1000x magnification.

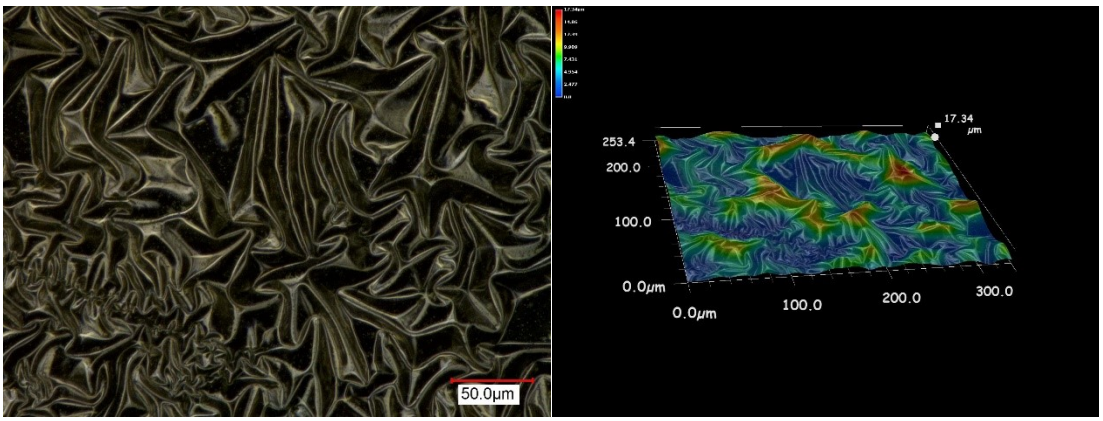

Fig. 12 *Image of the sample´s surface (left), and 3D surface´s image (right) of sample B_0,8_G.*

The Fig. 12 shows a uniform surface of the glossy wrinkled PPy layer, which occurs at the sample prepared with the highest concentration of Py solution (B_0,8_G).

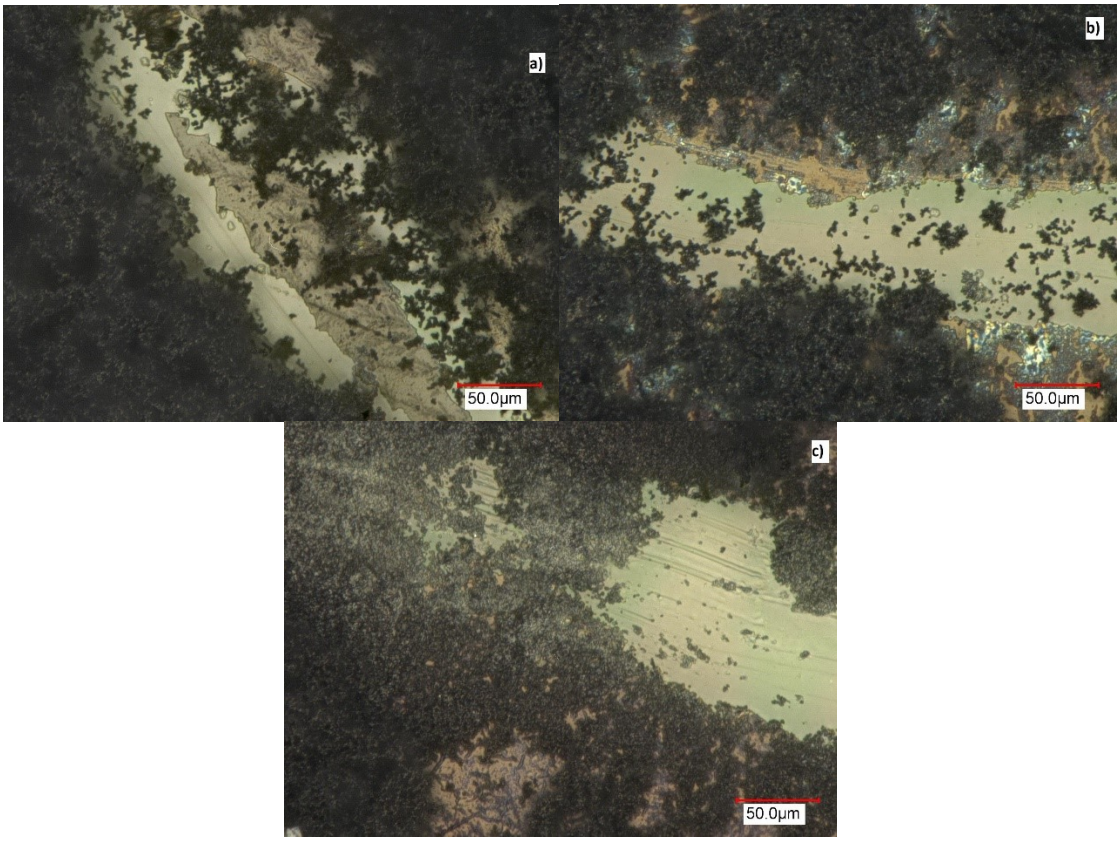

Fig. 13 *Pictures of D series of samples prepared on the PET foil substrate; a) The sample D_0,15_PET; b) The sample D_0,4_PET; c) The sample D_0,8 PET.*

Samples were measured at 1000x magnification. Unlike the series of samples prepared on the glass, there is only a little visible difference between the concentrations of the starting Py solutions. Again, there is a wrinkled layer on the samples, which in this case is not as glossy as at the samples prepared on the glass. The amount of dendritic PPy is very similar in all samples prepared on the PET substrate (Fig. 13).

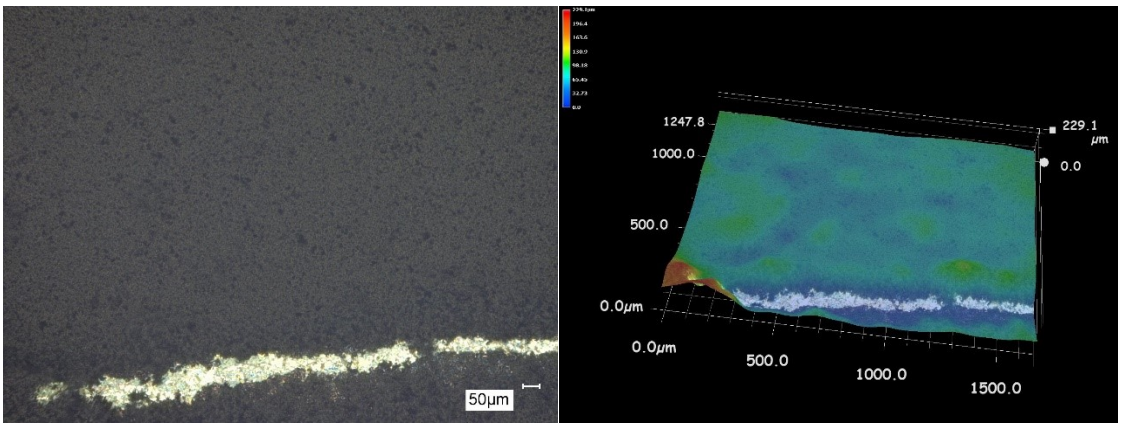

Fig. 14 *Picture of the surface of the sample E_0,15_Si (left); the 3D image of the sample´s surface (right).*

The layer made on the Si wafer substrate appears to be much smoother compared to the samples made on the glass. Again, there is a wrinkled layer on which is a shrub PPy. This image (Fig. 14) was taken with only 200 times magnification.

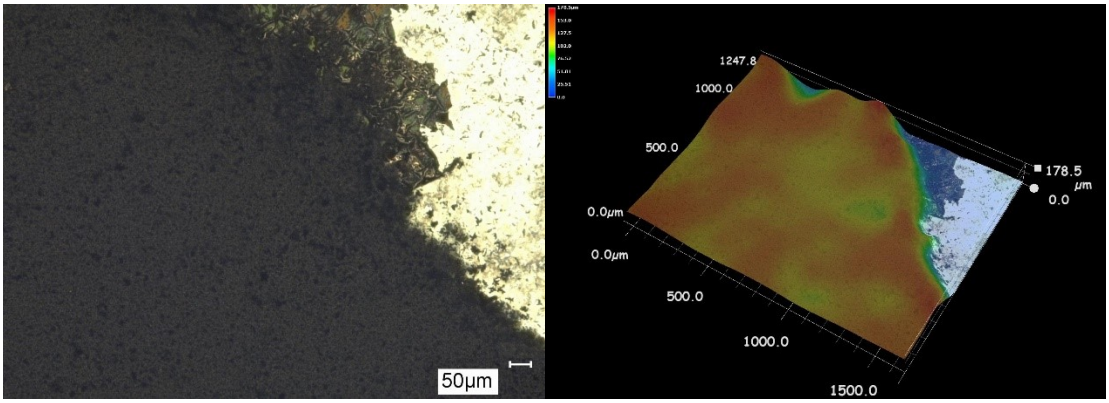

Fig. 15 *Picture of the surface of the sample E_0,4_Si (left); the 3D image of the sample´s surface (right).*

In comparison with the samples on a glass substrate, the layer can be easily “wiped” from the Si wafer substrate. The wrinkled layer is visible at the edges of the scratch, otherwise, it is completely homogeneously covered with dendritic PPy (Fig. 15). In this measurement, the magnification was also 200x.

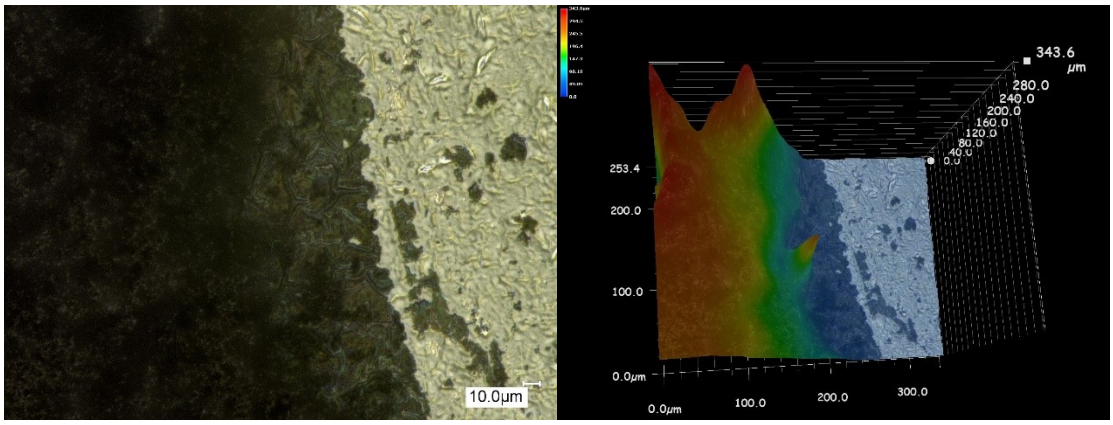

Fig. 16 *Picture of the surface of the sample E_0,8_Si (left); the 3D image of the sample´s surface (right).*

Unlike the previous two samples, this measurement was performed at a 1000 times magnification. On the far right (on the picture of the sample´s surface), the Si wafer surface itself is visible, on which, more to the left, there is visible a wrinkled layer. On the far left can be seen the dendritic PPy (Fig. 16).

The 3D images of the surface of prepared samples are in full resolution enclosed in Attachment B.

Raman spectroscopy: Average values of measured Raman scattering spectra of the prepared layers were compared for the individual concentration (of Py solution) values. In one figure, the spectra of one concentration, for each used substrate – glass (conductive and non-conducting samples), PET foils, and the silicon wafer, are compared. Table 3 shows measured wavenumbers of all measured series of samples.

Table 3 *Measured wavenumbers of all measured series of samples.*

A series of samples			B series of samples			D series of samples			E series of samples				
0,15	**0,4**	**0,8**	**0,15**	**0,4**	**0,8**	**0,15**	**0,4**	**0,8**	**0,15**	**0,4**	**0,8**	$\left[\frac{mol}{dm^3}\right]$	
930	927	927	937	938	938	948	926	940	933	929	930	[cm^{-1}]	A
969	968	968	977	979	976	976	988	980	972	969	969		B
1049	1049	1049	1056	1058	1058	1053	1063	1059	1075	1068	1064		C
									1075	1085	1082		
1250	1249	1245	1259	1261	1253				1241	1245	1246		D
1354	1361	1374	1347	1344	1340	1370	1387	1344	1377	1372	1370		E
1582	1577	1576	1586	1587	1588	1583	1585	1580	1587	1586	1585		F

A → C-C ring deformation (b); B → C-C ring in-plane deformation (p); C → Symmetric C-H in-plane bending, N-H in-plane deformation with radical cation (p); D → quinoid bipolaron structure (b); E → C-C in-ring, C-C inter-ring, C-N antisymmetric in-ring (o); F → C=C in-ring and C-C inter-ring in the backbone (o); p – polaron; b – bipolaron; o – overlapping of polaron and bipolaron.

The spectra contain characteristic bands for PPy. The main band of PPy is located at ~1580 cm^{-1} and is assigned to C=C in-ring and C-C inter-ring in the backbone and arises from polaron and bipolaron structures. Broadband in the range 1300 – 1400 cm^{-1} corresponds to the different pyrrole ring vibrations, which also is comprised with polaron and bipolaron structures 0[31]. Other broadband at ~1050 cm^{-1} belonged to symmetric C-H in-plane bending and N-H in-plane deformation with radical cation is caused by polaron structure in the PPy chain. Two bands below 1000 cm^{-1} (at ~930 cm^{-1} and ~970 cm^{-1}) are assigned to the C-C vibration in bipolaron and polaron structure, respectively. The conductivity of PPy can relate to the position of band belonging to vibration C=C/C-C (~1580 cm^{-1}) [32]. Lower wavenumber of the band should mean better conductivity. This statement is in accordance with conductivity measurements of samples on glass (A) and silicon (Si). However, comparison of all substrates did not fit.

All measured spectra show the very similar shape and bands ratios, but there are differences in case of samples on a glass substrate which are not conductive, where the band corresponding to the polaronic structure (~970 cm^{-1}) is slightly more intensive than a band of bipolaronic structure (~930cm^{-1}). For other sample series, glass (A), foil (D), and silicon (E), the most intensive is the band of bipolaronic structure or has the same intensity.

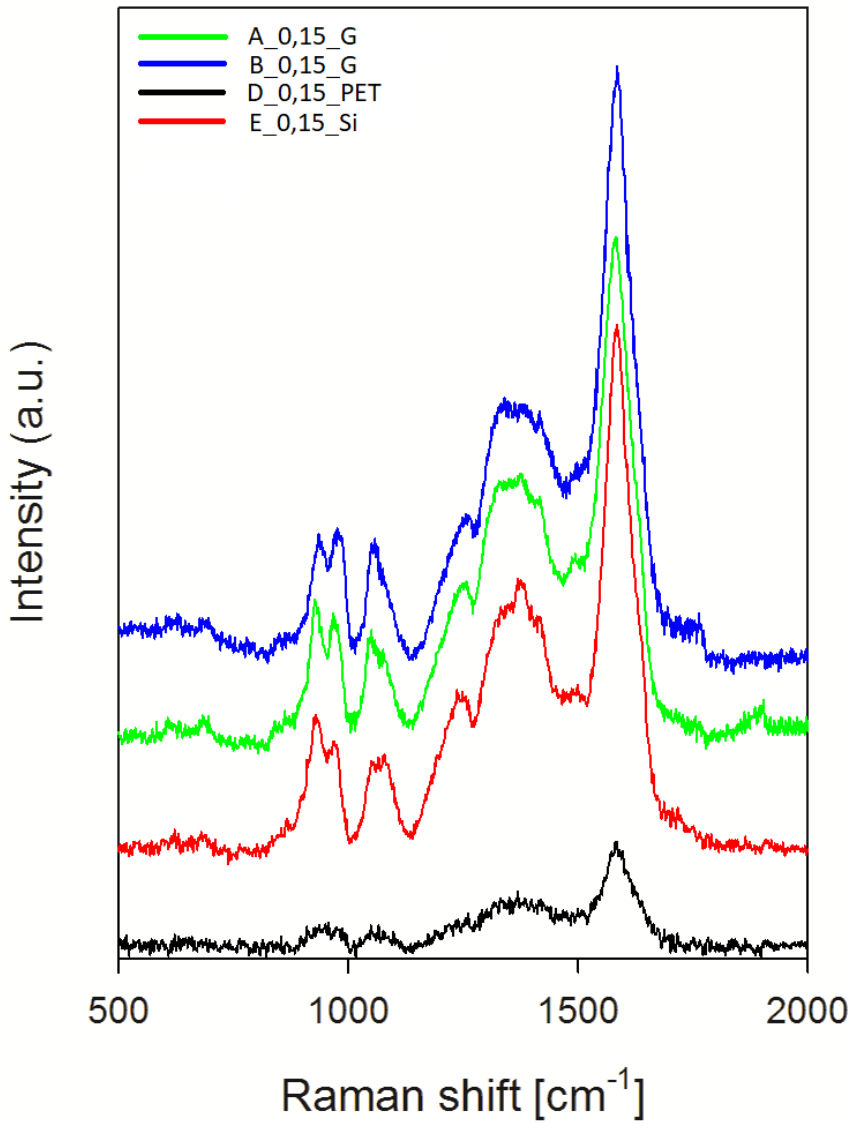

Fig. 17 *Raman spectra of samples A_0,15_G; B_0,15_G; D_0,15_PET; and E_0,15_Si.*

In the Fig. 17 the major peak on the right relates to the conductivity of PPy (~1580 cm^{-1}) [32]. It shows, in agreement with conductivity measurement, that sample on the PET substrate is the least conductive, but for non-conductive sample, it shows the same intensity as well conductive samples (on glass and Si wafer). Spectra on foil substrate are very noisy, which should be probably connected with the substrate and/or with the thickness of the layer on the substrate. The noise of the spectra is also possibly connected with missing band at ~1250 cm^{-1} (quinoid bipolaron structure) [31].

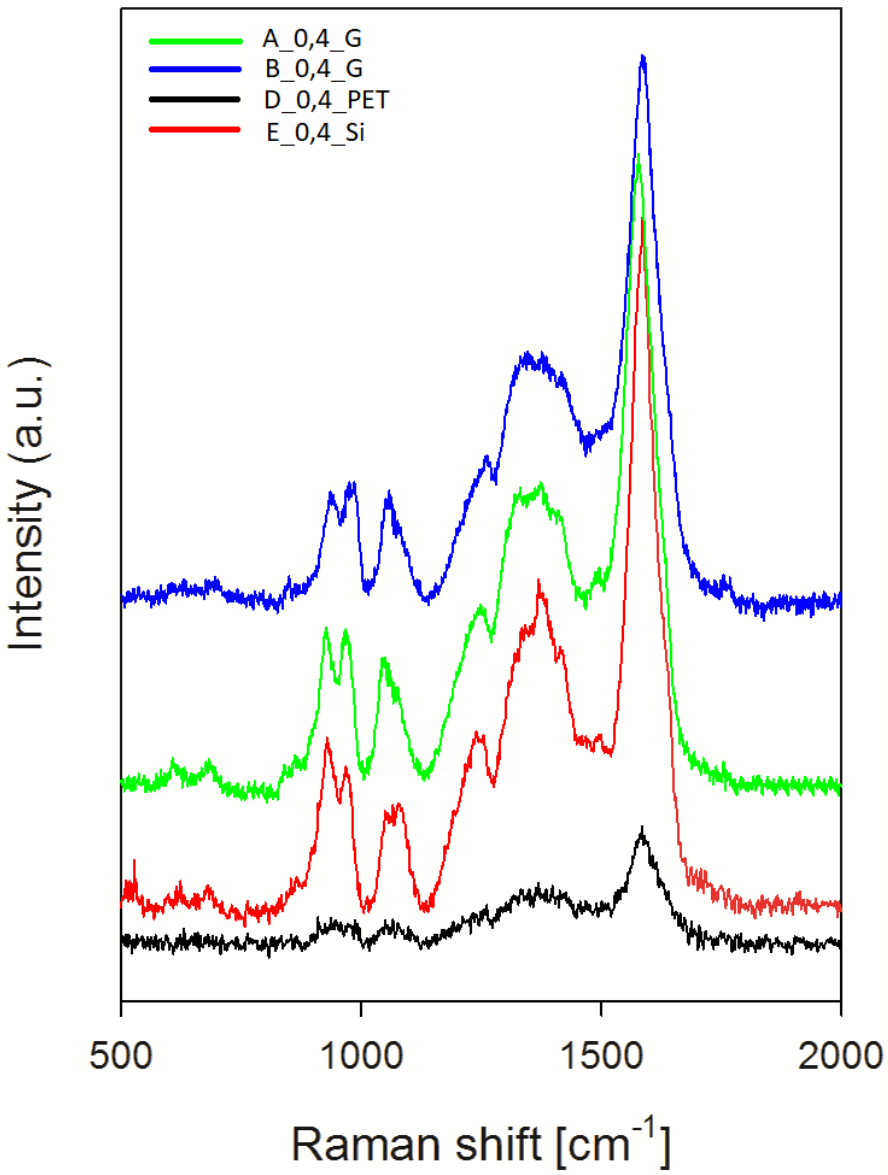

Fig. 18 Raman spectra of samples A_0,4_G; B_0,4_G; D_0,4_PET; and E_0,4_Si.

The Fig. 18 shows the same phenomena at non-conductive sample as the previous one. The band connected with conductivity seems to have the biggest intensity for the sample prepared on Si wafer substrate.

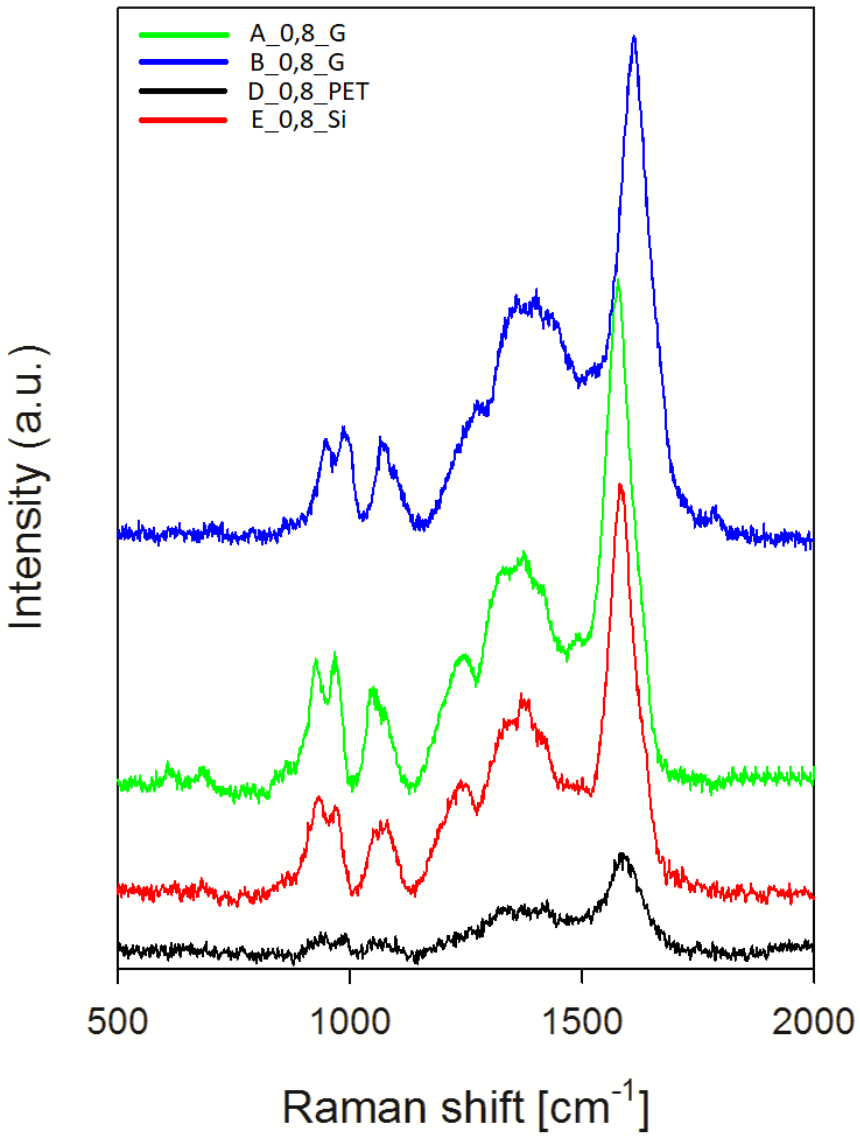

Fig. 19 Raman spectra for samples A_0,8_G; B_0,8_G; D_0,8_PET; and E_0,8_Si.

The band corresponding to the polaron structure (~970 cm^{-1}) is slightly more intensive, for non-conductive sample (all in the B series) than a band of bipolaron structure (~930cm^{-1}). For samples on other substrates, glass (A), foil (D), and silicon wafer (E), the most intensive is the band of bipolaron structure or has the same intensity as the band of polaron structure. From this can be said that the ratio of polarons and bipolarons of the wrinkled layer, which can be found without dendritic PPy only on non-conductive samples, and the ratio of polarons and bipolarons of the layers containing both the wrinkled layer and the dendritic PPy is opposite.

Raman spectroscopy measurements should provide results that could support conductivity measurements in case of non-conductive samples. Unfortunately, the

position of the band connected with conductivity did not bring anything relevant to infer the results, because it´s intensity was on the same level that for well conducting samples. The measurement was also carried out on the surface´s spots where was only the wrinkled layer or only the dendritic PPy. Unfortunately, the comparison of these measurements did not provide any useful information. From the bipolaron and polaron band ratios, the comparison always came out the same way, only the non-conducting layers on glass have the opposite ratio of those two. Regarding the position of the band, which could indicate the conductivity, there was nothing interesting about what could be leaned and somehow inferred the results. If we wanted to continue with the study then, much more measurement would have to be done and it would be for a more thorough study.

3.3.2 Results of molecular modeling

Models studied using molecular modeling differed by the position of PPy chains relative to the substrate. The Fig. 20 shows PET substrate with one marked PET chain to show how the positions of PPy chains were divided on the substrate.

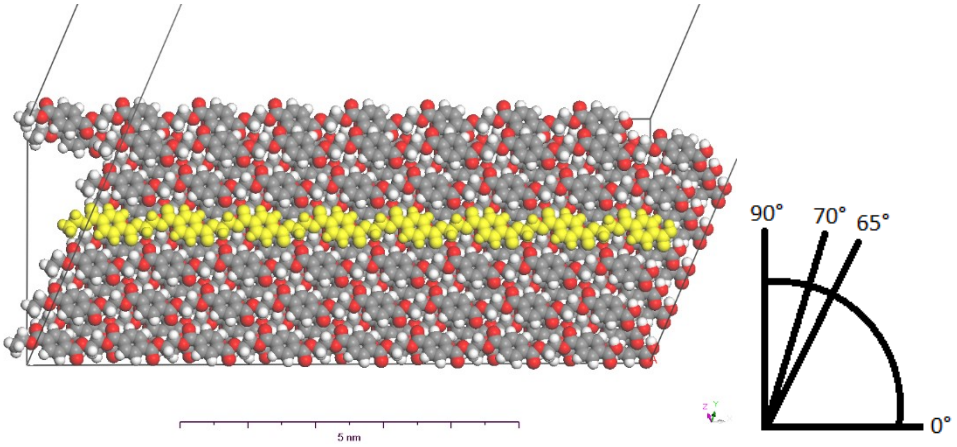

Fig. 20 *Model of PET substrate with a highlighted molecule of PET chain. The division into categories according to tilt angles between PPy and PET (PPy/PET).*

The positions of PPy chains on PET substrate were divided into 4 categories according to the angle between the highlighted molecule of PET chain and inserted molecules of PPy, i.e. 0°, 65°, 70°, and 90°. The position on 65° corresponds to the position of the PPy chain lying only on benzene rings (for more molecules of PPy, each one lies on

the separated line of benzene ring). The 70° position differs from the 65° by the placement of PPy chain on the functional groups with oxygen. The graph in Fig. 21 corresponds to energies of the optimized models of PET with 1, 3, and 4 PPy chains. It contains average values for interaction energies for each category.

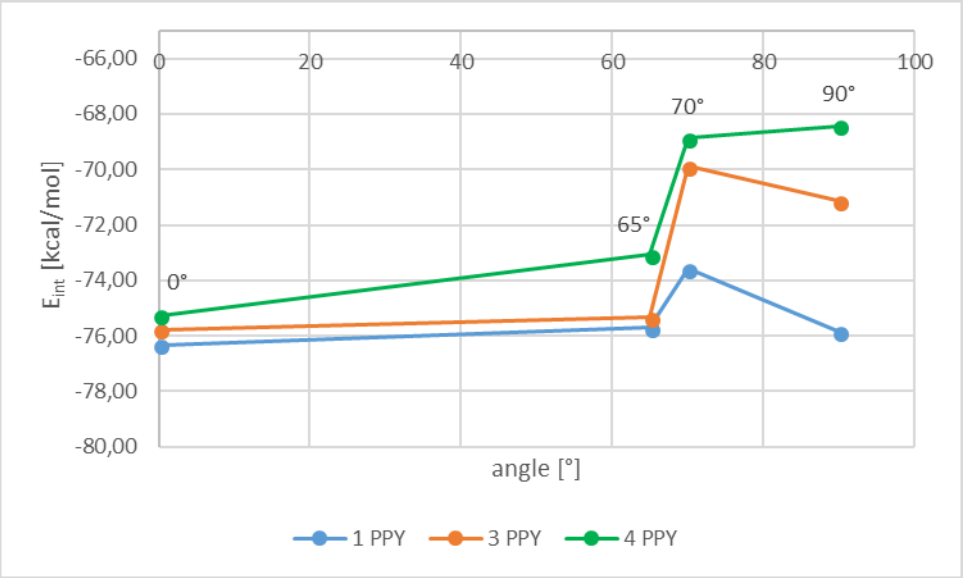

Fig. 21 *Energy dependence on the angle between PPy/PET.*

The chart shows the same trend for all models (with 1, 3 or 4 PPy chains) – models with PPy chains parallel to the PET chains are in comparison with models with angled PPy slightly better. Values used in the chart in Fig. 21 are summarized in Table 4.

Table 4 *Summarized average values of interaction energies for series of models on PET.*

Angle PPy/PET [°]	1 PPY; E_{int} [kcal/mol]	3 PPY; E_{int} [kcal/mol]	4 PPY; E_{int} [kcal/mol]
0	-76,34	-75,77	-75,28
65	-75,71	-75,33	-73,08
70	-73,59	-69,89	-68,88
90	-75,84	-71,14	-68,43

Models of silicon wafer substrate were also divided into 4 categories depending on the angle between the substrate and PPy chains. Fig. 22 and Fig. 23 show the 0° angle and 90° angle, respectively. The direction of the visible rows of Si atoms is (0 1 1).

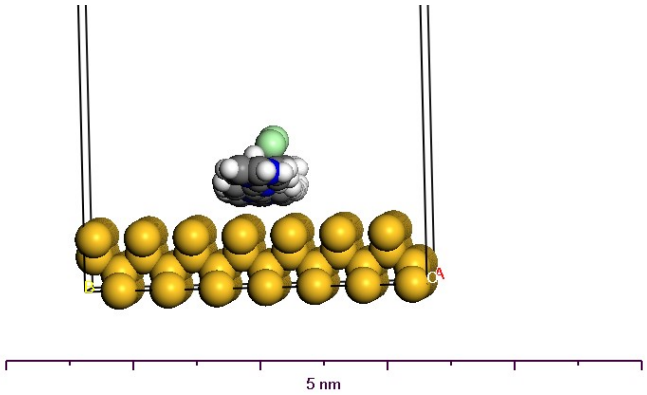

Fig. 22 *Model of Si substrate with PPy chain in 0° position.*

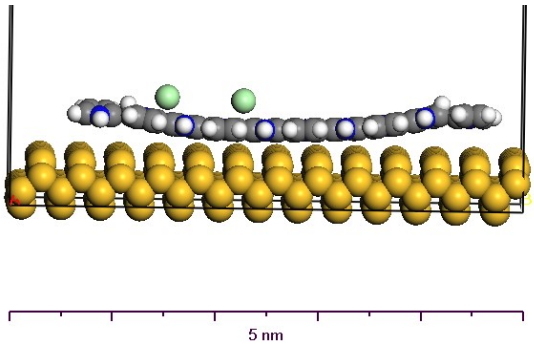

Fig. 23 *Model of Si substrate with PPy chain in 90° position.*

It means that in 0° category, PPy chain is parallel to the direction of the rows, and in the case of 90° category, it is perpendicular to this direction. The other two categories were 30° and 70°. They were obtained from placing the PPy chain diagonally on a rectangular substrate. The chart in Fig. 24 shows average values of interactive energies of the optimized models for Si substrate for 1, 3, and 4 PPy chains.

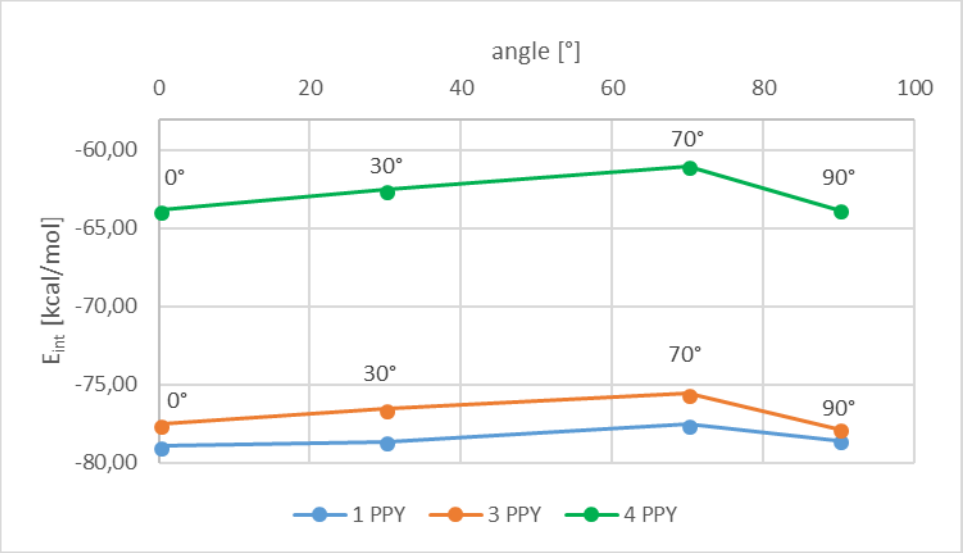

Fig. 24 *Energy dependence on the angle between PPy chains and rows on Si substrate.*

According to the chart in Fig. 24 can be said that models with PPy parallel or perpendicular to the rows are slightly more energy efficient than those at an angle of 30° or 70°. The difference increases with increasing number of PPy chains, however, it can be concluded that the change of E_{int} in dependence of angle is negligible. Values used in the graph in Fig. 24 are summarized in Table 5. The interaction energy increases with more molecules of PPy because there is also a mutual interaction between the chains which occurs in all prepared models on all substrates containing more than 1 PPy chain. In comparison with PET substrate, the scattering of values is greater in the case of PET substrate which is also more sensitive to the position of PPy chains on the substrate. This sensitivity to the positioning can relate to the lowest measured conductivity. Attachment of PPy chains to the benzene rings or functional groups with oxygen plays a key role in the case of PET substrate – individual positions on the substrate are not equivalent. On the contrary, Si substrate is not that sensitive to the changes of the position of PPy chains like PET substrate, however, little differences can be observed. The differences between the position of molecules of PPy is very small.

Table 5 *Summarized average values of interaction energies for series of models on Si.*

Angle PPy/rows [°]	1 PPY; E_{int} [kcal/mol]	3 PPY` E_{int} [kcal/mol]	4 PPY` E_{int} [kcal/mol]
0	-78,94	-77,54	-63,85
30	-78,65	-76,57	-62,54
70	-77,54	-75,56	-61,03
90	-78,56	-77,85	-63,82

Since the glass is amorphous and does not have any periodicity (except for the periodicity imposed by periodic condition of the cell), the PPy chains were placed on it only randomly. There is a visible drop in interaction energy which is caused by interactions between the chains itself like on other substrates. Soda lime glass substrate model was also compared with a substrate made from quartz glass structure (obtained from structure library of Materials Studio) that does not contain any free ions, unlike soda lime glass. In Table 6 are compared average values of interaction energies of prepared models with 1, 3 and 4 PPy chains on a glass substrate, and with 1 PPy chain on a quartz glass substrate.

Table 6 *Summation of average values of interaction energies for models on glass and quartz substrate.*

model	E_{int} [kcal/mol]	average deviation
1PPy – glass	-180,45	34,45
1PPy – quartz glass	-93,83	11,84
3PPy – glass	-144,00	25,72
4PPy – glass	-136,67	25,45

From values listed in Table 6 is obvious that ions and non-saturated oxygens contained in soda lime glass substrate have a huge influence on interaction energy which is higher in comparison to the quartz glass model even for models containing more than one PPy chain. Since the Si wafer substrate and PET foil neither contain ions, in terms of adhesion, the layers they less stick to these substrates, which I also felt when preparing and working with prepared layers. The Attachment A contains models with lowest interaction energy for all groups of models.

3. Conclusion

In my work I successfully prepared polypyrrole layers on three different substrates. Prepared samples were analysed by Optical microscopy which showed that the formed layers consist of two "subunits" – wrinkled layer (connected directly to the substrate´s surface) and dendritic polypyrrole attached to the wrinkled layer. The dendritic polypyrrole was not present only on B series of samples, which differed from A series of samples by the position of the substrate in the preparation process. The B series also did not show any conductivity in the conductivity measurements which indicates that the dendritic polypyrrole can have great influence in terms of conductivity. The D series of samples prepared on the polyethylene terephthalate substrate showed the lowest conductivity from the conductive samples which was in accordance with the results of Raman spectroscopy analysis. However, the results of Raman spectroscopy did not bring any information that could infer the results for the B series of samples in case of conductivity, because the Raman spectra show the band, related to the polypyrrole conductivity, with the same intensity for both the conductive and non-conductive samples. In further analysis, I have compiled a series of atomistic models that compare used substrates in terms of interaction energy of the layer with the substrate. The results show that position of the polypyrrole chains relative to the substrate has grater impact in case of the polyethylene terephthalate foil substrate in comparison to other substrates. The position of the molecules of polypyrrole also has an impact in case of the Si wafer substrate, but it is not as high as on the foil substrate. The glass substrate is amorphous, so it does not provide any other possibilities of arrangement than according to the outer boundary of the model (cell structure). The prepared glass substrate was compared with the SiO_2 quartz glass structure obtained from Materials Studio library. This comparison showed that free ions and non-saturated atoms of oxygen have great impact to the interaction energy, because the interaction energy is lowest for models prepared on the glass substrate. Unfortunately, I was not able to correctly explain the deviation in data obtained for non-conducting layers which gives the opportunity to follow up on this work in subsequent research.

Literature

[1] GOTTWALD, Tomáš. Vodivé polymery a jejich využití v superkondenzátorech: Conducting polymers and their use in supercapacitors [CD-ROM]. Brno: Vysoké učení technické, Fakulta elektrotechniky a komunikačních technologií, 2010. 57s Diplomová práce.

[2] VERNITSKAYA, Tat'yana V a Oleg N EFIMOV. Polypyrrole: a conducting polymer; its synthesis, properties and applications. *Russian Chemical Reviews* [online]. 1997, 66(5), 443-457. DOI: 10.1070/RC1997v066n05ABEH000261. ISSN 0036021x.

[3] JATRATKAR, Aviraj A., Jyotiprakash B. YADAV, Sandip V. KAMAT, Vaishali S. PATIL, D.B. MAHADIK, Harish C. BARSHILIA, Vijaya PURI a R.K. PURI. Consequence of oxidant to monomer ratio on optical and structural properties of Polypyrrole thin film deposited by oxidation polymerization technique. *Journal of Physics and Chemistry of Solids* [online]. 2015, 80, 78-83. DOI: 10.1016/j.jpcs.2015.01.004. ISSN 00223697. Dostupné z:http://linkinghub.elsevier.com/retrieve/pii/S0022369715000050

[4] ATES, Murat, Tolga KARAZEHIR a A. SEZAI SARAC. Conducting Polymers and their Applications. Current Physical Chemistry [online]. 2012, 2(3), 224-240. DOI: 10.2174/1877946811202030224. ISSN 18779468.

[5] PRATESI, Pietro, Sui neri di pirrolo, *Gazzett Chimica Italiana*, 67, 188 (1937)

[6] PROKEŠ, Jan, Jaroslav STEJSKAL a Mária OMASTOVÁ. Polyanilin apolypyrrol - dva představitelé vodivých polymerů. Chemické listy. 2001, 95(8), 484-492.

[7] KANAZAWA, K. Keiji, A. F. DIAZ, Roy H. GEISS, William D. GILL, James F. KWAK, J. Anthony LOGAN, John F. RABOLT a G. Bryan STREET. Organic metals: polypyrrole, a stable synthetic 'metallic' polymer. J. Chem. Soc., Chem. Commun [online]. 1979, (19), 854-855. DOI: 10.1039/C39790000854. ISSN 0022-4936. Dostupné z: http://xlink.rsc.org/?DOI=C39790000854

[8] ZOTTI, G. a G. SCHIAVON. Spectroclectrochemical determination of polarons in polypyrrole and polyaniline. Synthetic Metals [online]. 1989, 30(2), 151-158. DOI: 10.1016/0379-6779(89)90785-6. ISSN 03796779. Dostupné z: http://linkinghub.elsevier.com/retrieve/pii/0379677989907856

[9] WALLER, Andrew M. a Richard G. COMPTON. Simultaneous alternating current impedance/electron spin resonance study of electrochemical doping in polypyrrole. Journal of the Chemical Society, Faraday Transactions 1: Physical Chemistry in Condensed Phases [online]. 1989, 85(4), 977-. DOI: 10.1039/f19898500977. ISSN 0300-9599. Dostupné z: http://xlink.rsc.org/?DOI=f19898500977

[10] DIAZ, A. F., K. Keiji KANAZAWA a Gian Piero GARDINI. Electrochemical polymerization of pyrrole. *Journal of the Chemical Society, Chemical Communications* [online]. 1979, (14), 635-. DOI: 10.1039/c39790000635. ISSN 0022-4936. Dostupné z: http://xlink.rsc.org/?DOI=c39790000635

[11] SHINDE, Sujata S., Girish S. GUND, Vijay S. KUMBHAR, Bebi H. PATIL a Chandrakant D. LOKHANDE. Novel chemical synthesis of polypyrrole thin film electrodes for supercapacitor application. European Polymer Journal [online]. 2013, 49(11), 3734-3739. DOI: 10.1016/j.eurpolymj.2013.07.032. ISSN 00143057.
Dostupné z: http://linkinghub.elsevier.com/retrieve/pii/S0014305713003893

[12] HUANG, Z., P-C WANG, J. FENG, A.G. MACDIARMID, Y. XIA a G.M. WHITESIDES. Selective deposition of films of polypyrrole, polyaniline and nickel on hydrophobic/hydrophilic patterned surfaces and applications. Synthetic Metals [online]. 1997, 85(1-3), 1375-1376. DOI: 10.1016/S0379-6779(97)80279-2. ISSN 03796779. Dostupné z: http://linkinghub.elsevier.com/retrieve/pii/S037967799780279 2K

[13] THOMPSON, Brianna C., Simon E. MOULTON, Rachael T. RICHARDSON a Gordon G. WALLACE. Effect of the dopant anion in polypyrrole on nerve growth and release of a neurotrophic protein. *Biomaterials* [online]. 2011, **32**(15), 3822-3831. DOI: 10.1016/j.biomaterials.2011.01.053. ISSN 01429612. Dostupné z: http://linkinghub.elsevier.com/retrieve/pii/S0142961211000822

[14] BANIASADI, Hossein, Ahmad RAMAZANI S. A, Shohreh MASHAYEKHAN, Marzieh Ramezani FARANI, Fariba GHADERINEZHAD a Mohammadhossein DABAGHI. Design, Fabrication, and Characterization of Novel Porous Conductive Scaffolds for Nerve Tissue Engineering. *International Journal of Polymeric Materials and Polymeric Biomaterials* [online]. 2015, 64(18), 969-977. DOI: 10.1080/00914037.2015.1038817. ISSN 00914037. Dostupné z: http://www.tandfonline.com/doi/full/10.1080/00914037.2015.1038817

[15] NOUFI, Rommel. Protection of Semiconductor Photoanodes with Photoelectrochemically Generated Polypyrrole Films. Journal of The Electrochemical Society [online]. 1981, 128(12), 2596-. DOI: 10.1149/1.2127298. ISSN 00134651. Dostupné z: http://jes.ecsdl.org/cgi/doi/10.1149/1.2127298

[16] ALMUNTASER, Faisal M. A., Sutripto MAJUMDER, Prashant K. BAVISKAR, Jaydeep V. SALI a B. R. SANKAPAL. Synthesis and characterization of polypyrrole and its application for solar cell. Applied Physics A [online]. 2017, 123(8), -. DOI: 10.1007/s00339-017-1131-y. ISSN 0947-8396. Dostupné z: http://link.springer.com/10.1007/s00339-017-1131-y

[17] HINCHLIFFE, Alan. Molecular modelling for beginners. Hoboken, NJ: Wiley, c2003. ISBN 0470843101.

[18] RAPPE, A. K., C. J. CASEWIT, K. S. COLWELL, W. A. GODDARD a W. M. SKIFF. UFF, a full periodic table force field for molecular mechanics and molecular dynamics simulations. Journal of the American Chemical Society [online]. 1992, 114(25), 10024-10035. DOI: 10.1021/ja00051a040. ISSN 0002-7863. Dostupné z: http://pubs.acs.org/doi/abs/10.1021/ja00051a040

[19] SHOENBERG, Ronald. Optimization with the Quasi-Newton Method [online]. Aptech Systems, Inc. Maple Valley, WA, 2001 [cit. 2018-05-12]. Dostupné z: http://www.aptech.com/wp-content/uploads/2013/05/qnewton.pdf

[20] GASTEIGER, Johann a Mario MARSILI. Iterative partial equalization of orbital electronegativity—a rapid access to atomic charges. Tetrahedron [online]. 1980, 36(22), 3219-3228. DOI: 10.1016/0040-4020(80)80168-2. ISSN 00404020. Dostupné z: http://linkinghub.elsevier.com/retrieve/pii/0040402080801682

[21] RAPPE, Anthony K. a William A. GODDARD. Charge equilibration for molecular dynamics simulations. The Journal of Physical Chemistry [online]. 1991, 95(8), 3358-3363. DOI: 10.1021/j100161a070. ISSN 0022-3654. Dostupné z: http://pubs.acs.org/doi/abs/10.1021/j100161a070

[22] NAVALE, S.T., A.T. MANE, M.A. CHOUGULE, R.D. SAKHARE, S.R. NALAGE a V.B. PATIL. Highly selective and sensitive room temperature NO2 gas sensor based on polypyrrole thin films. Synthetic Metals [online]. 2014, 189, 94-99. DOI: 10.1016/j.synthmet.2014.01.002. ISSN 03796779. Dostupné z: http://linkinghub.elsevier.com/retrieve/pii/S0379677914000058

[23] WANG, Pen-Cheng a Jing-Yu YU. Dopant-dependent variation in the distribution of polarons and bipolarons as charge-carriers in polypyrrole thin films synthesized by oxidative chemical polymerization. Reactive and Functional Polymers [online]. 2012, 72(5), 311-316. DOI: 10.1016/j.reactfunctpolym.2012.03.005. ISSN 13815148. Dostupné z: http://linkinghub.elsevier.com/retrieve/pii/S1381514812000600

[24] DIAS, H.V. Rasika, Mauro FIANCHINI a R.M. Gamini RAJAPAKSE. Greener method for high-quality polypyrrole. Polymer [online]. 2006, 47(21), 7349-7354. DOI: 10.1016/j.polymer.2006.08.033. ISSN 00323861. Dostupné z: http://linkinghub.elsevier.com/retrieve/pii/S0032386106009876

[25] JOSHI, Aditee, S.A. GANGAL a S.K. GUPTA. Ammonia sensing properties of polypyrrole thin films at room temperature. Sensors and Actuators B: Chemical [online]. 2011, 156(2), 938-942. DOI: 10.1016/j.snb.2011.03.009. ISSN 09254005. Dostupné z: http://linkinghub.elsevier.com/retrieve/pii/S092540051100205X

[26] KARMAKAR, N., R FERNANDES, Shilpa JAIN, U.V. PATIL, Navinchandra G. SHIMPI, N.V. BHAT a D.C. KOTHARI. Room temperature NO 2 gas sensing properties of p-toluenesulfonic acid doped silver-polypyrrole nanocomposite. Sensors and Actuators B: Chemical [online]. 2017, 242, 118-126. DOI: 10.1016/j.snb.2016.11.039. ISSN 09254005. Dostupné z: http://linkinghub.elsevier.com/retrieve/pii/S0925400516318305

[27] TSE, John S. a Thomas C. W. MAK. Refinement of the crystal structure of polyethylene terephthalate. Journal of Crystal and Molecular Structure [online]. 1975, 5(1), 75-80. DOI: 10.1007/BF01202554. ISSN 0308-4086. Dostupné z: http://link.springer.com/10.1007/BF01202554

[28] CORMACK, A.N. a Jincheng DU. Molecular dynamics simulations of soda–lime–silicate glasses. Journal of Non-Crystalline Solids [online]. 2001, 293-295, 283-289. DOI: 10.1016/S0022-3093(01)00831-6. ISSN 00223093. Dostupné z: http://linkinghub.elsevier.com/retrieve/pii/S0022309301008316

[29] MACEŠKA, R. Měření vodivosti kapalin. Brno: Vysoké učení technické v Brně, Fakulta elektrotechniky a komunikačních technologií, 2009. 73s. Vedoucí bakalářské práce doc. Ing. Petr Beneš, Ph.D.

[30] TABAČIAROVÁ, Jana, Matej MIČUŠÍK, Pavol FEDORKO a Mária OMASTOVÁ. Study of polypyrrole aging by XPS, FTIR and conductivity measurements. Polymer Degradation and Stability [online]. 2015, 120, 392-401. DOI: 10.1016/j.polymdegradstab.2015.07.021. ISSN 01413910. Dostupné z: http://linkinghub.elsevier.com/retrieve/pii/S0141391015300537

[31] SU, N., H. B. LI, S. J. YUAN, S. P. YI a E. Q. YIN. Synthesis and characterization of polypyrrole doped with anionic spherical polyelectrolyte brushes. Express Polymer Letters [online]. 2012, 6(9), 697-705. DOI: 10.3144/expresspolymlett.2012.75. ISSN 1788618X. Dostupné z: http://www.expresspolymlett.com/letolt.php?file=EPL-0003325&mi=c

[32] CHEN, Wei, Chang Ming LI, Peng CHEN a C.Q. SUN. Electrosynthesis and characterization of polypyrrole/Au nanocomposite. Electrochimica Acta [online]. 2007, 52(8), 2845-2849. DOI: 10.1016/j.electacta.2006.07.005. ISSN 00134686. Dostupné z: http://linkinghub.elsevier.com/retrieve/pii/S0013468606007183

Acknowledgements

In the first place, I would like to thank Assoc. Prof. Ing. Lenka Kulhánková, Ph.D., and Assoc. Prof. Ing. Jonáš Tokarský, Ph.D., for their professional guidance, help and effort they put in me. I hope they were pleased with results of this work and with my effort. I would also like to thank Mgr. Pavlína Peikertová, Ph.D., for performed analysis of Raman spectroscopy and optical microscopy and her help with evaluation of the results of analysis; to Ing. Petra Vilímová for measurement of layers‘ thickness. Research described in this master thesis has been supported by the Ministry of Education, Youth and Sports of the Czech Republic within SGS (projects reg. no. SP2017/6 and SP2018/95). I also thank for the National Sustainability Program II (NPU II) “IT4Innovations excellence in science” (project reg. no. LQ1602)